Aerospace Science and Technology 82–83 (2018) 105–118

Contents lists available at ScienceDirect

Aerospace Science and Technology

www.elsevier.com/locate/aescte

Cooperative aerial lift and manipulation (CALM)

Hossein Rastgoftar *, Ella M. Atkins

Aerospace Engineering Department, University of Michigan, Ann Arbor, MI, USA

ARTICLE INFO

Article history:
Received 30 April 2018
Received in revised form 4 September 2018
Accepted 4 September 2018
Available online 10 September 2018

Keywords:
Scalability
Customizability
Manipulation
Locomotion
Planning
Unmanned aerial vehicles

ABSTRACT

This paper proposes a novel paradigm for aerial payload transport and object manipulation by an unmanned aerial vehicle (UAV) team. This new paradigm, called *cooperative payload lift and manipulation* (CALM), applies the continuum deformation agent coordination approach to transport and manipulate objects autonomously with collision avoidance guarantees. CALM treats UAVs as moving supports during transport and as stationary supports during object manipulation. Constraints are formulated to assure sufficient thrust forces are available to maintain stability and follow prescribed motion and force/torque profiles. CALM uses tensegrity muscles to carry a suspended payload or a manipulation object rather than cables. A tensegrity structure is lightweight and can carry both the tension and compression forces required during cooperative manipulation. During payload transport, UAVs are categorized as leaders and followers. Leaders define continuum deformation shape and motion profile while followers coordinate through local communication. Each UAV applies input–output (IO) feedback linearization control to track the trajectory defined by continuum deformation. For object manipulation, the paper proposes a new hybrid force controller to stabilize quadcopters when smooth or sudden (impulsive) forces and moments are exerted on the system.

1. Introduction

Natural disasters such as earthquakes, wildfires, and hurricanes have created devastating disaster zones where survival relies on emergency responder support. Access roads in disaster zones may be covered with debris or destroyed, making it difficult for survivors to access supplies such as clean water, food, and medicine even after the supplies have been delivered to the greater region. Small UAVs (unmanned aerial vehicles) offer an alternative to manned helicopters that can act as a force multiplier for supply delivery in disaster zones. A team of small UAVs can carry an appreciable package and can be flexibly deployed from local supply stations to maneuverably transport payload to people in need.

This paper develops the underlying theory to enable *cooperative payload transport* in support of disaster relief and other missions requiring payload carriage through a constrained environment with unimproved launch and delivery sites. Because a small UAV team will need to potentially pickup and manipulate its payload at each remote site, this paper also develops a theory for *cooperative object manipulation*. Because cable and tether systems can only support tension loads, this work presumes a lightweight tensegrity structure replaces the cable connecting UAV and payload so that the UAV team can provide the required tension and compression forces to achieve the required payload (grasping) manipulation forces and torques. The proposed multi-UAV system provides a comprehensive capability we denote Cooperative Aerial Lift and Manipulation (CALM).

Manipulation Robots (MRs) are now able to accomplish a variety of tasks that include but are not limited to grasping, pushing, sliding, tipping, rolling, and throwing. Although MRs can have multiple degrees of freedom, the number of robots collaboratively directing a single manipulation task has been limited in previous work. Furthermore, most MRs require grounding or connection to a grapple fixture. Our goal is to assemble and coordinate many UAVs as stable supports for aerial object manipulation in environments difficult to access or stabilize with ground-based manipulation. In this manner, objects can be grappled, released, and manipulated, enabling the UAV team to clear debris, pick up and deploy supply packages, or perform repairs or construction tasks given appropriate manipulation tooltip designs.

Relevant background and contributions are presented below. Mathematical preliminaries are followed by a problem statement and specification for the CALM system. Transport and stationary support MUS (multi UAV system) control strategies are presented and analyzed, and simulation results are presented to illustrate and evaluate the CALM specification.

* Corresponding author.
E-mail addresses: hosseinr@umich.edu (H. Rastgoftar), ematkins@umich.edu (E.M. Atkins).

https://doi.org/10.1016/j.ast.2018.09.005

1.1. Background

Cooperative control of multiple unmanned aerial vehicles (UAVs) has been an active area of research for over two decades. Formation flight [1], air traffic control [2], transportation engineering [3], aerobiological sampling of agricultural lands [4], cooperative manipulation [5] and general team-based surveillance are some applications of UAV cooperative control. A UAV team can improve mission efficiency, reduce cost, and offer increased resilience to failures including individual UAV loss. Group cooperation also improves fault detection and ability for the team to recover from anomaly conditions [6,7]. Coordination of a multi-agent system (MAS) using Laplacian control has been considerably studied over the last decade [7]. Laplacian control methods include consensus algorithms [8–12] and partial differential equation (PDE) methods [13–15]. A containment approach [16–20] to coordination has also been proposed. Consensus is the most common approach used for distributed control in multi-agent systems. Consensus has been applied for distributed motion control [21–24], distributed sensing [25,10], medical applications [26], and power distribution systems [27,28].

In containment control multiple leaders guide the MAS toward a desired target shape using consensus to update positions [29, 30,19,16]. Go-Stop hybrid control strategies in [20,30] enable the leaders to guide followers to a desired target. Containment control under fixed and switching MAS communication topologies are developed in [31,32]. Containment control of a MAS formation modeled as double integrators was presented in [18]. Additionally, containment control with complex communication weights was investigated in [18]. MAS containment control under directed communication topology was studied in [33,34], event-based containment control of multi-agent systems was defined in [35,31], and finite-time containment control of a multi-agent system is studied in [36,37].

UAVs have been applied in payload transport, grasping and manipulation tasks. These tasks require UAVs to manage total forces and moments applied to external object(s) along with their collective motions. Manipulation can be used to achieve perching or deploy/pickup payloads, or the cooperative team can carry slung loads [38,39]. Swing-free trajectory tracking is demonstrated by a single quadcopter carrying a payload in [40]. Aerial manipulation using a single quadcopter is studied in [41]. Ref. [42] shows how multiple quadcopters can participate in a cooperative manipulation task. Stabilization of a helicopter carrying a payload is studied in [43,44]. In Ref. [45,46] stabilization of a single quadcopter carrying a single payload is analyzed. The connecting cable between each UAV and the slung payload is modeled by serially-connected bar elements in [45]. Ref. [46] assumes that the cable is active only if it is taut. Ref. [46] proposes a differentially flat hybrid controller to stabilize a slung payload with a single quadcopter.

Modeling and control of multiple UAVs deployed for cooperative manipulation are investigated in [47,41,5], while cooperative grasping of a payload using multiple UAVs is studied in [48,47]. Adaptive control for a slung load transport mission using a single rotorcraft is studied in [49–51]. Stability of a slung load carried by multiple single-rotor helicopters is investigated in [52], while an inverse kinematics formulation for aerial payload transport is presented in [53]. Cooperative manipulation and transportation with three quadcopters are modeled and experimentally demonstrated in [3]. Refs. [54,55] suggests a geometric control scheme to control payload transport with multiple UAVs.

1.2. Contribution

The proposed *Cooperative Aerial Lift and Manipulation* (CALM) system offers payload transport and object manipulation capabilities. The multi-UAV (unmanned aerial vehicle) system (MUS) and tensegrity [56] structure tethering system are the main CALM elements. The MUS contains a large number of small unmanned aerial vehicles (UAVs) that provide moving supports for payload transport. Each tensegrity arm is comprised of a finite set of tensegrity muscles. A tensegrity muscle consists of a finite number of tensegrity prism cells, where each prism cell is made of tethers and rigid bars. A tensegrity arm is lightweight but sufficiently stiff to carry tension and compression forces.

The first contribution of this paper is to characterize and enhance manipulation **deformability** and **scalability**. The paper applies the principles of continuum mechanics to coordinate CALM UAVs in a three-dimensional motion space [57]. Because continuum deformation is homeomorphic, no two separate particles of a continuum (or deformable body) occupy the same position in a continuum deformation, and inter-agent distances can significantly change. Treating UAV coordination as continuum deformation, we formally verify safety by providing inter-agent collision avoidance guarantees [57]. By ensuring inter-agent collision avoidance through continuum deformation coordination, a large number of UAVs can participate in a CALM mission. Increasing the number of support UAVs offers the following advantages: (i) Manipulation cost is manageable (low) while efficiency and robustness increase. (ii) Fault-tolerance and reconfiguration capabilities in a cooperative manipulation mission are improved. (iii) UAVs collectively carry nontrivial payloads while MUS coordination maneuverability is improved. (iv) Because inter-agent distances can be expanded or contracted via continuum deformation, the UAV team can navigate constrained environments including passing through a narrow channel. This paper shows how a desired continuum deformation can be acquired by support UAVs in real-time through local communication with minimal computation overhead.

CALM supports customized operation modes of the MUS, offering **Customizability** as the second paper contribution. A MUS can act either as moving supports in a payload transport mission or as stationary supports in an object manipulation scenario. The proposed CALM system can successfully accomplish two main tasks in a cooperative fashion that include:

- Transportation tasks in which CALM carries a common tethered payload from an initial location to a target destination. In a transportation mission, support UAVs must be able to carry rigid and deformable payloads and avoid collision with obstacles. This work presumes a tensegrity structure connecting each UAV to the common payload.
- Force control mode in which external forces exerted on UAV supports can be either smooth or impulsive. The CALM force control system must deal with discontinuous forces including contact and impulse forces, as well as continuous forces. We propose a hybrid control model to stabilize MUS when they act in stationary support model for an object manipulation task.

Decentralized payload transport is the third contribution of the paper. Compared to related work [54], one CALM advantage is that agent coordination is acquired through local communication in real-time with less computation cost. To the best of our knowledge, available cooperative payload transport work relies on centralized coordination approaches. Ref. [54] applies the Lagrange method to calculate quadcopter desired thrust force in a centralized fashion. Given a desired trajectory for the slung payload, Ref. [54] then applies the virtual structure method to coordinate UAVs. Our work instead assumes that each UAV is equipped with a force sensor to measure and indirectly regulate tensegrity muscle force at any time t. Given force sensor readings, each UAV assigns the control thrust force in real-time to achieve a desired trajectory assigned by local communication.

This paper is organized as follows. Preliminary graph theory notions, a background on continuum deformation coordination, and position notations are presented in Section 2. The problem statement in Section 3 is followed by the CALM system mathematical model in Section 4. CALM control systems including position control and hybrid force control (HFC) are modeled in Section 5. In Sections 6 and 7, we describe how quadcopters can act as moving supports in a payload transport task, or as stationary supports in an object manipulation scenario. Stability of MUS-payload system is discussed in Section 8. Simulation results presented in Section 9 are followed by concluding remarks in Section 10.

2. Preliminaries

2.1. Graph theory notions

Let collective motion in a $3D$ space be decomposed into a $2D$ continuum deformation in the X–Y plane and a $1D$ continuum deformation along the Z axis. The graph $\mathcal{G}$ defines inter-agent communication in the X–Y plane. The graph $\mathcal{G}=\mathcal{G}(\mathcal{V},\mathcal{E},\mathcal{W})$ is a weighted digraph defining inter-agent communication for a quadcopter team. Further, $\mathcal{V}=\{1,2,\cdots,N\}$ is the node set, where $i\in\mathcal{V}$ represents a quadcopter's index number. Three quadcopters, defining a $2D$ continuum deformation, are called *leaders*. The remaining quadcopters are called *followers*. Leader quadcopter index numbers are defined by $\mathcal{V}_L=\{1,2,3\}$, and follower quadcopter index numbers are defined by $\mathcal{V}_F=\{4,5,\cdots,N\}$. The edge set $\mathcal{E}\subset\mathcal{V}\times\mathcal{V}$ defines communication among quadcopters. The set $\mathcal{N}_i=\{j\,|\,(j,i)\in\mathcal{E}_{CD}\}$ defines in-neighbor quadcopters of a quadcopter i. Leader quadcopters are assumed to move independently. Thus, $\mathcal{N}_i=\emptyset$, if $i\in\mathcal{V}_L$. The set $\mathcal{W}:\mathcal{E}\to(0,1)$ defines follower communication weights.

2.2. Position terminology

It is assumed that position is expressed with respect to a fixed *ground coordinate system*. The unit bases of the ground coordinate system are mutually orthogonal and denoted $\hat{\mathbf{e}}_1$, $\hat{\mathbf{e}}_2$, and $\hat{\mathbf{e}}_3$. The **actual position of quadcopter** i is denoted $\mathbf{r}_i=x_i\hat{\mathbf{e}}_1+y_i\hat{\mathbf{e}}_2+z_i\hat{\mathbf{e}}_3$. **Initial position of quadcopter** i is denoted by $\mathbf{R}_i=X_i\hat{\mathbf{e}}_1+Y_i\hat{\mathbf{e}}_2+Z_i\hat{\mathbf{e}}_3$. We define

$$\mathcal{Y}_i=x_i\hat{\mathbf{e}}_1+y_i\hat{\mathbf{e}}_2 \tag{1}$$

as the **actual output of quadcopter** i. The **global desired output of quadcopter** i is given by a continuum deformation in the X–Y plane and denoted by

$$\mathcal{Y}_{i,HT}=x_{i,HT}\hat{\mathbf{e}}_1+y_{i,HT}\hat{\mathbf{e}}_2. \tag{2}$$

The **local desired position of quadcopter** i is given by

$$\mathcal{Y}_{d,i}=\begin{cases}\mathcal{Y}_{i,HT} & i\in\mathcal{V}_L\\ \sum_{j\in\mathcal{N}_i}w_{i,j}\mathcal{Y}_j & i\in\mathcal{V}_F\end{cases}. \tag{3}$$

Note that $w_{i,j}$ is the communication weight of follower i with agent j. $w_{i,j}$ is positive if $j\in\mathcal{N}_i$; otherwise, it is zero. In Section 2.3.2, communication weight characteristic equations are obtained; communication weights are consistent with agents' positions at initial time t_0. If followers apply the communication weights given in Section 2.3.2 a MQS continuum deformation will be prescribed.

Remark. At initial time t_0, actual, local and global desired outputs are identical: $[X_i\ Y_i]^T=\mathcal{Y}_i(t_0)=\mathcal{Y}_{i,HT}(t_0)=\mathcal{Y}_{d,i}(t_0)$.

This paper assumes the payload is a rigid body with an arbitrary orientation in a 3-D motion space. Therefore, payload configuration is specified at any time t only by knowing three unique points of the payload known as *payload characteristic points*. Payload characteristic points are denoted O_1, O_2, and O_3. The **actual position** of payload characteristic point O_k is denoted $\mathbf{r}_{O_k}=x_{O_k}\hat{\mathbf{e}}_1+y_{O_k}\hat{\mathbf{e}}_2+z_{O_k}\hat{\mathbf{e}}_3$ $(k=1,2,3)$. Payload characteristic points form a rigid triangle in the motion space.

2.3. Continuum deformation background

2.3.1. Continuum deformation definition

By definition, a continuum is a domain consisting of an infinite number of particles with infinitesimal size. [58]. This paper considers a class of continuum deformation called *homogeneous transformation*, given by

$$\mathcal{Y}_{i,HT}(t)=Q(t)\mathbf{R}_i+\mathbf{D}(t), \tag{4}$$

where $Q\in\mathbb{R}^{3\times3}$ is the Jacobian matrix, $\mathbf{r}_{i,HT}(t)$ is the global desired position of quadcopter i initially positioned at $\mathbf{R}_i$. Also, $\mathbf{D}=[D_1\ D_2\ D_3]^T$ is the rigid-body displacement vector. This paper assumes the MQS deforms in the X–Y plane, so

$$Q=\begin{bmatrix}Q_{\mathrm{CD}} & \mathbf{0}\\ \mathbf{0} & 1\end{bmatrix}=\begin{bmatrix}Q_{1,1} & Q_{1,2} & 0\\ Q_{2,1} & Q_{2,2} & 0\\ 0 & 0 & 1\end{bmatrix}. \tag{5}$$

Elements of Q_{CD} $(Q_{1,1}, Q_{1,2}, Q_{2,1}, Q_{2,2})$, D_1 and D_2 can be defined based on the positions of the leaders [57]:

$$\begin{bmatrix}Q_{1,1}(t)\\Q_{1,2}(t)\\Q_{2,1}(t)\\Q_{2,2}(t)\\D_1(t)\\D_2(t)\end{bmatrix}=\begin{bmatrix}X_1 & Y_1 & 0 & 0 & 1 & 0\\X_2 & Y_2 & 0 & 0 & 1 & 0\\X_3 & Y_3 & 0 & 0 & 1 & 0\\0 & 0 & X_1 & Y_1 & 0 & 1\\0 & 0 & X_2 & Y_2 & 0 & 1\\0 & 0 & X_3 & Y_3 & 0 & 1\end{bmatrix}\begin{bmatrix}x_{1,HT}(t)\\x_{2,HT}(t)\\x_{3,HT}(t)\\y_{1,HT}(t)\\y_{2,HT}(t)\\y_{3,HT}(t)\end{bmatrix}. \tag{6}$$

Polar decomposition of the continuum deformation Jacobian matrix Using polar decomposition, Q_{CD} can be expressed as

$$Q_{\mathrm{CD}}=\mathcal{R}_{\mathrm{CD}}U_{\mathrm{CD}}, \tag{7}$$

where U_{CD} is a positive definite (and symmetric) matrix and $\mathcal{R}_{\mathrm{CD}}$ is an orthogonal matrix, e.g $\mathcal{R}_{\mathrm{CD}}^T\mathcal{R}_{\mathrm{CD}}=I_2$. Eigenvalues of matrix U_{CD} are positive and real and denoted by λ_1 and λ_2 $(0<\lambda_1\le\lambda_2)$.

Key feature of a homogeneous transformation: It is assumed that the three leaders are non-aligned at all times t. Therefore,

$$\forall t\ge t_0,\qquad \mathrm{Rank}\left[\mathbf{r}_{2,HT}-\mathbf{r}_{1,HT}\quad \mathbf{r}_{3,HT}-\mathbf{r}_{1,HT}\right]=2. \tag{8}$$

The three leaders form a *leading triangle* in the X–Y plane. Under a homogeneous transformation, X and Y components of the global desired position of quadcopter $i\in\mathcal{V}$ can be expressed as in [57]:

$$t\ge t_0,\qquad \mathcal{Y}_{i,HT}=\begin{bmatrix}x_{i,HT}(t)\\y_{i,HT}(t)\end{bmatrix}=\sum_{j=1}^{3}\alpha_{i,j}\begin{bmatrix}x_{j,HT}(t)\\y_{j,HT}(t)\end{bmatrix}, \tag{9}$$

where $\alpha_{i,1}$, $\alpha_{i,2}$, and $\alpha_{i,3}$ are **time-invariant** parameters and $\alpha_{i,1}+\alpha_{i,2}+\alpha_{i,3}=1$. $\alpha_{i,1}$, $\alpha_{i,2}$, are $\alpha_{i,3}$ are computed from quadcopter i initial position and the three leaders as follows [57]:

$$\begin{bmatrix}X_1 & X_2 & X_3\\Y_1 & Y_2 & Y_3\\1 & 1 & 1\end{bmatrix}\begin{bmatrix}\alpha_{i,1}\\\alpha_{i,2}\\\alpha_{i,3}\end{bmatrix}=\begin{bmatrix}X_i\\Y_i\\1\end{bmatrix}. \tag{10}$$

2.3.2. Continuum deformation acquisition

Continuum deformation is acquired by followers through local communication. Inter-agent communication is defined by a weighted graph with the following properties [57]:

1. Follower quadcopter i interacts with three in-neighbor quadcopters defined by the set $\mathcal{N}_i = \{i_1, i_2, i_3\}$.
2. In-neighbor quadcopters' initial positions satisfy the following rank condition:

$$\text{Rank}\begin{bmatrix}\mathbf{R}_{i_2}-\mathbf{R}_{i_1} & \mathbf{R}_{i_3}-\mathbf{R}_{i_1}\end{bmatrix}=2. \quad (11)$$

An example continuum deformation communication graph is shown in Fig. 2.

3. Given initial positions of quadcopter $i \in \mathcal{V}_F$ and i_1, i_2, i_3, denoted by $\mathbf{R}_i$, $\mathbf{R}_{i_1}$, $\mathbf{R}_{i_2}$, and $\mathbf{R}_{i_3}$, communication weights are obtained from

$$\begin{bmatrix} X_{i_1} & X_{i_2} & X_{i_3} \\ Y_{i_1} & Y_{i_2} & Y_{i_3} \\ 1 & 1 & 1 \end{bmatrix}\begin{bmatrix} w_{i,i_1} \\ w_{i,i_2} \\ w_{i,i_3}\end{bmatrix} = \begin{bmatrix} X_i \\ Y_i \\ 1\end{bmatrix}. \quad (12)$$

The last row of Eq. (12) ensures $w_{i,i_1}+w_{i,i_2}+w_{i,i_3}=1$. Note that w_{i,i_1}, w_{i,i_2}, and w_{i,i_3} are positive because quadcopter $i \in \mathcal{V}_F$ is inside the triangle defined by the in-neighbor agents.

We can set up a weight matrix $W \in \mathbb{R}^{(N-3)\times N}$ with the ij entry defined as follows:

$$W_{ij} = \begin{cases} w_{i+3,j} & i+2 \in \mathcal{V}_F,\ j \in \mathcal{N}_{i+3} \\ -1 & j = i+3 \\ 0 & \text{else} \end{cases}. \quad (13)$$

Let $W = [B\ \ A]$, where $B \in \mathbb{R}^{(N-3)\times 3}$ is the leader-follower communication matrix and $A \in \mathbb{R}^{(N-3)\times(N-3)}$ is the follower-follower communication matrix. The follower-follower communication matrix A has the following properties [57]:

1. All diagonal entries of the matrix A are -1.
2. Off-diagonal elements of A are non-negative.
3. The matrix A is Hurwitz.

With communication weights assigned by Eq. (12), quadcopter X and Y position components satisfy the following:

$$q = X, Y, \qquad A\begin{bmatrix} q_4 & \cdots & q_N\end{bmatrix}^T + B\begin{bmatrix} q_1 & q_2 & q_3\end{bmatrix}^T = \mathbf{0}.$$

Therefore,

$$q = X, Y, \qquad \begin{bmatrix} q_4 & \cdots & q_N\end{bmatrix}^T = W_L\begin{bmatrix} q_1 & q_2 & q_3\end{bmatrix}^T,$$

where

$$W_L = -A^{-1}B = \begin{bmatrix} \alpha_{4,1} & \alpha_{4,2} & \alpha_{4,3} \\ \vdots & \vdots & \vdots \\ \alpha_{N,1} & \alpha_{N,2} & \alpha_{N,3}\end{bmatrix}, \quad (14)$$

$\alpha_{i,1}$, $\alpha_{i,2}$, and $\alpha_{i,3}$ are the α parameters satisfying Eq. (10).

3. Problem statement

Consider a CALM system with the schematic shown in Fig. 3. The CALM structure consists of five main elements:

- **MUS**: It is assumed that a MUS consists of N multicopters cooperating as moving or stationary supports for the CALM structure (See Fig. 3 (a,b)).

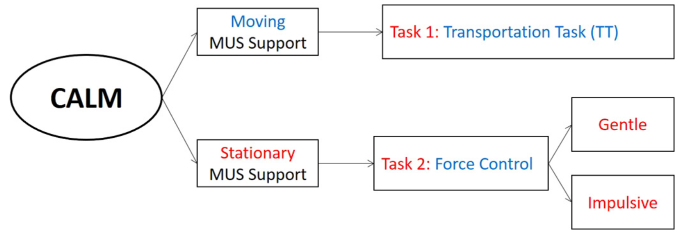

Fig. 1. CALM operation modes.

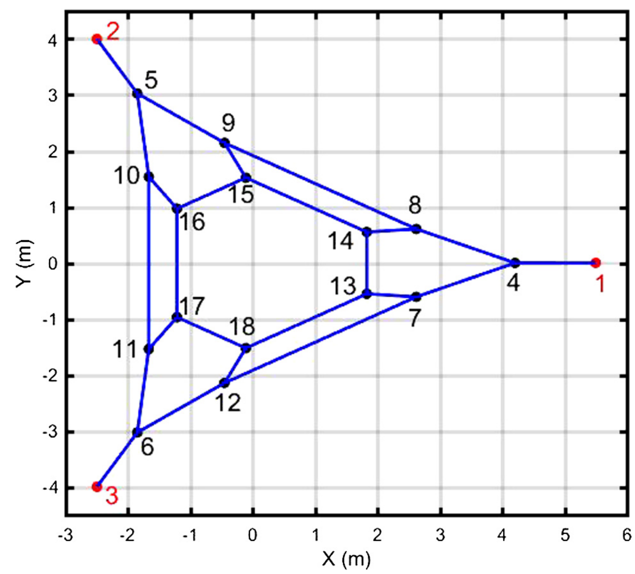

Fig. 2. Inter-agent communication graph used by followers to acquire the desired continuum deformation.

- **Tensegrity arm**: Each tensegrity arm consists of a finite number of tensegrity muscles. A tensegrity muscle is made of serially-connected prism tensegrity cells [56]. Schematic of a prism tensegrity cell is shown in Fig. 3(c). Each prism cell is made of bars and tethers. A tensegrity muscle can carry both tension and compression forces.
- **Gripper**: A tensegrity arm is connected to a distinct gripper; each is commanded by a spiral motor.
- **Mechanical joints**: To avoid topological obstructions, tensegrity muscles are attached to a multicopter and a gripper or fixture by a three-DOF revolute wrist.
- **Payload**: The payload can be either a rigid or deformable body. It can be a live creature (e.g. such as a human or animal) or a rigid object that should be transported between two locations. Note the payload object can be a single manipulator with multiple degrees of freedom to maximize manipulation capability.

As shown in Fig. 1, a CALM mission can support two primary tasks: (i) Transportation Task (TT) and (ii) Force Control (FC). In TT, the MUS carries a payload. Therefore, the UAVs act as moving supports of the CALM system.

For FC, the MUS provides stationary supports of the tensegrity arms carrying a single/multiple degree of freedom manipulation system. During FC, the forces and moments applied by the grippers to a fixture or payload can be either smooth or impulsive. Note that gentle forces and moments exerted on the grippers are not necessarily continuous but they are also not harsh and impulsive.

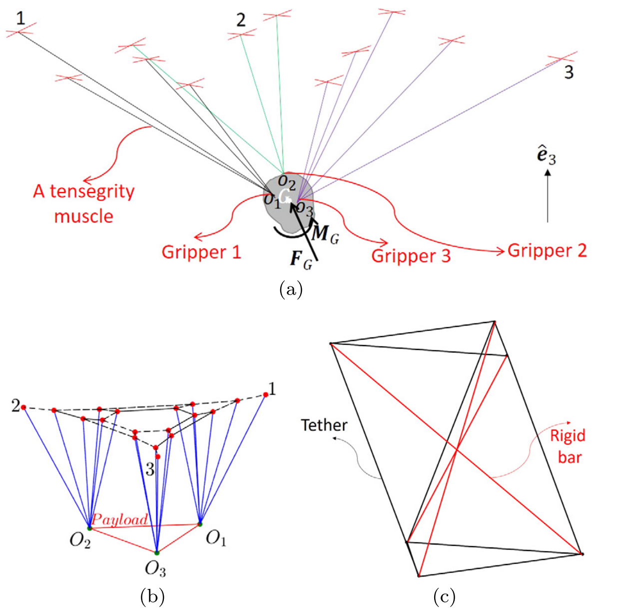

Fig. 3. (a) Schematic of a CALM system carrying a payload. (b) Simulation example of the CALM structure with three grippers O_1, O_2, and O_3. (c) Schematic of a tensegrity prism cell with bar elements and tethers. A tensegrity prism cell is made of three bars and nine tensile elements.

4. CALM system mathematical model

4.1. UAV model

Assume a MAS consisting of N quadcopters moves as a group in a 3-D motion space. The dynamics of quadcopter $i \in \mathcal{V}$ is given by

$$\dot{\mathbf{r}}_i = \mathbf{v}_i$$

$$\dot{\mathbf{v}}_i = \begin{bmatrix} 0 \\ 0 \\ -g \end{bmatrix} + \bar{F}_{T,i} \begin{bmatrix} C_{\phi_i} S_{\theta_i} C_{\psi_i} + S_{\phi_i} S_{\psi_i} \\ C_{\phi_i} S_{\theta_i} S_{\psi_i} - S_{\phi_i} C_{\psi_i} \\ C_{\phi_i} C_{\theta_i} \end{bmatrix} + \bar{\mathbf{F}}_{\text{EXT},i}, \tag{15}$$

$$\begin{bmatrix} \ddot{\bar{F}}_{T,i} & \ddot{\phi}_i & \ddot{\theta}_i & \ddot{\theta}_i \end{bmatrix}^T = \begin{bmatrix} u_{T,i} & u_{\phi,i} & u_{\theta,i} & u_{\psi,i} \end{bmatrix}^T$$

where ϕ_i, θ_i, ψ_i are quadcopter i roll, pitch, and yaw angles, $\mathbf{r}_i = x_i\hat{\mathbf{e}}_1 + y_i\hat{\mathbf{e}}_2 + z_i\hat{\mathbf{e}}_3$, $\mathbf{v}_i = v_{x,i}\hat{\mathbf{e}}_1 + v_{y,i}\hat{\mathbf{e}}_2 + v_{z,i}\hat{\mathbf{e}}_3$, $g = 9.81$ m/s^2 is the gravity, $\bar{F}_{\text{EXT},i} = \frac{F_{\text{EXT},i}}{m_i}$ is the external force per unit mass, $\bar{F}_{T,i} = \frac{F_{T,i}}{m_i}$ is the thrust force per unit mass, and m_i is the quadcopter mass. Furthermore, $u_{T,i}$, $u_{\phi,i}$, $u_{\theta,i}$, and $u_{\psi,i}$ are the control inputs. Note that $C_{(.)}$ and $S_{(.)}$ are the abbreviations for cos(.) and sin(.), respectively.

The rotational dynamics of quadcopter i is given by [59]

$$\begin{bmatrix} T_{\phi,i} \\ T_{\theta,i} \\ T_{\psi,i} \end{bmatrix} = \begin{bmatrix} I_{xx,i} & 0 & 0 \\ 0 & I_{yy,i} & 0 \\ 0 & 0 & I_{zz,i} \end{bmatrix} \times \left(\mathcal{R}_{\omega,i} \begin{bmatrix} \ddot{\phi}_i \\ \ddot{\theta}_i \\ \ddot{\psi}_i \end{bmatrix} + \dot{\mathcal{R}}_{\omega,i} \begin{bmatrix} \dot{\phi}_i \\ \dot{\theta}_i \\ \dot{\psi}_i \end{bmatrix} + I_{r,i} \begin{bmatrix} \omega_{x,i} \\ \omega_{y,i} \\ 0 \end{bmatrix} \omega_{\Gamma,i} \right) - \begin{bmatrix} (I_{zz,i} - I_{yy,i}) (\dot{\theta}_i C_{\phi_i} + \dot{\psi}_i C_{\theta_i} S_{\phi_i}) (-\dot{\theta}_i S_{\phi_i} + \dot{\psi}_i C_{\theta_i} C_{\phi_i}) \\ (I_{xx,i} - I_{zz,i}) (\dot{\phi}_i - \dot{\psi}_i S_{\theta_i}) (-\dot{\theta}_i S_{\phi_i} + \dot{\psi}_i C_{\theta_i} C_{\phi_i}) \\ (I_{yy,i} - I_{xx,i}) (\dot{\phi}_i - \dot{\psi}_i S_{\theta_i}) (\dot{\theta}_i C_{\phi_i} + \dot{\psi}_i C_{\theta_i} S_{\phi_i}) \end{bmatrix}, \tag{16}$$

where

$$\mathcal{R}_{\omega,i} = \begin{bmatrix} 1 & 0 & -\sin\theta_i \\ 0 & \cos\phi_i & \cos\theta_i \sin\phi_i \\ 0 & -\sin\phi_i & \cos\theta_i \cos\phi_i \end{bmatrix}. \tag{17}$$

Note that $\ddot{\phi}_i = u_{\phi,i}$, $\ddot{\theta}_i = u_{\theta,i}$, and $\ddot{\psi}_i = u_{\psi,i}$ in Eq. (16) are substituted by u_{ϕ_i}, u_{θ_i}, and u_{ψ_i} assigned in Section 5. Also, $\omega_{\Gamma,i} = \omega_{1,i} - \omega_{2,i} + \omega_{3,i} - \omega_{4,i}$, where $\omega_{1,i}$ through $\omega_{4,i}$ are the angular speeds of rotors 1, 2, 3, and 4 uniquely related to $F_{T,i}$, $T_{\phi,i}$, $T_{\theta,i}$, and $T_{\psi,i}$ (See Ref. [59]).

4.2. Tensegrity muscle

The paper assumes tensegrity muscle $i \in \mathcal{V}$ has negligible mass, so muscle i is a two-force member with stiffness k_i ($\frac{\text{N}}{\text{m}}$) and structural damping c_i ($\frac{\text{N.s}}{\text{m}}$). Tensegrity muscle i can carry both tension and compression forces. Each tensegrity muscle connects to a unique attachment point on the payload. Let payload connecting points be denoted O_1, O_2, and O_3. Then, $\zeta : \mathcal{V} \to \{O_1, O_2, O_3\}$ assigns a connecting point to each quadcopter $i \in \mathcal{V}$. Let $\zeta_i = \zeta(i)$ ($i \in \mathcal{V} \to \{O_1, O_2, O_3\}$). Then,

$$\bar{\mathbf{F}}_{\text{Muscle},i} = \frac{k_i}{m_i} \left(l_i - L_{f,i} \right) \mathbf{n}_i + \frac{c_i}{m_i} \begin{bmatrix} \dot{x}_{\zeta_i} - \dot{x}_i \\ \dot{y}_{\zeta_i} - \dot{y}_i \\ \dot{z}_{\zeta_i} - \dot{z}_i \end{bmatrix}, \tag{18}$$

where $l_i = \sqrt{\left(x_i - x_{\zeta_i}\right)^2 + \left(y_i - y_{\zeta_i}\right)^2 + \left(z_i - z_{\zeta_i}\right)^2}$, $L_{f,i}$ is the free length of muscle i, and $\mathbf{n}_i = \frac{[(x_{\zeta_i} - x_i) \ (y_{\zeta_i} - y_i) \ (z_{\zeta_i} - z_i)]^T}{l_i}$. Throughout the paper, we assume that $\bar{\mathbf{F}}_{\text{EXT},i} = \bar{\mathbf{F}}_{\text{Muscle},i}$ is the external force exerted on quadcopter i.

4.3. Payload dynamics

The MUS carries a 3-D payload with mass m_p. The principal body axes of the payload are denoted by $\hat{\mathbf{i}}_p$, $\hat{\mathbf{j}}_p$, and $\hat{\mathbf{k}}_p$. Define payload roll angle ϕ_p, payload pitch angle θ_p, and payload yaw angle ψ_p. These quantities are related to $\hat{\mathbf{e}}_1$, $\hat{\mathbf{e}}_2$, and $\hat{\mathbf{e}}_3$ by

$$\begin{bmatrix} \hat{\mathbf{i}}_b & \hat{\mathbf{j}}_b & \hat{\mathbf{k}}_b \end{bmatrix}^T = \mathcal{R}_p \begin{bmatrix} \hat{\mathbf{e}}_1 & \hat{\mathbf{e}}_2 & \hat{\mathbf{e}}_3 \end{bmatrix}^T, \tag{19}$$

where

$$\mathcal{R}_p = \begin{bmatrix} C_{\theta_p} C_{\psi_p} & C_{\theta_p} S_{\psi_p} & -S_{\theta_p} \\ S_{\phi_p} S_{\theta_p} C_{\psi_p} - C_{\phi_p} S_{\psi_p} & C_{\phi_p} C_{\psi_p} + S_{\phi_p} S_{\theta_p} S_{\psi_p} & S_{\phi_p} C_{\theta_p} \\ C_{\phi_p} S_{\theta_p} S_{\psi_p} + S_{\phi_p} S_{\psi_p} & C_{\phi_p} S_{\theta_p} S_{\psi_p} - S_{\phi_p} S_{\psi_p} & C_{\phi_p} C_{\theta_p} \end{bmatrix}. \tag{20}$$

The payload angular velocity is denoted by $\Omega_P = \omega_{x,p}\hat{\mathbf{i}}_p + \omega_{y,p}\hat{\mathbf{j}}_p + \omega_{z,p}\hat{\mathbf{k}}_p$, where $\omega_{x,p}$, $\omega_{y,p}$, and $\omega_{z,p}$ are related to $\dot{\phi}_p$, $\dot{\theta}_p$, and $\dot{\psi}_p$ by

$$\begin{bmatrix} \omega_{x,p} \\ \omega_{y,p} \\ \omega_{z,p} \end{bmatrix} = \begin{bmatrix} 1 & 0 & -\sin\theta_p \\ 0 & \cos\phi_p & \cos\theta_p \sin\phi_p \\ 0 & -\sin\phi_p & \cos\theta_p \cos\phi_p \end{bmatrix} \begin{bmatrix} \dot{\phi}_p \\ \dot{\theta}_p \\ \dot{\psi}_p \end{bmatrix}. \tag{21}$$

Payload mass moment of inertia values, expressed with respect to the payload body frame, are denoted by $I_{xx,p}$, $I_{yy,p}$, and $I_{zz,p}$. The quadcopters are connected to the payload at three connecting points O_1, O_2, and O_3. Define payload centroid position by $\mathbf{r}_p = x_p\hat{\mathbf{e}}_1 + y_p\hat{\mathbf{e}}_2 + z_p\hat{\mathbf{e}}_3$. Then the payload motion dynamics is modeled by

$$m_p \begin{bmatrix} \ddot{x}_p & \ddot{y}_p & \ddot{z}_p \end{bmatrix}^T = m_p \begin{bmatrix} 0 & 0 & -g \end{bmatrix}^T - \sum_{i=1}^{N} \mathbf{F}_{\text{Muscle},i} + \mathbf{F}_G, \tag{22a}$$

$$\begin{bmatrix} I_{xx,p}\dot{\omega}_{x,p} \\ I_{yy,p}\dot{\omega}_{y,p} \\ I_{zz,p}\dot{\omega}_{z,p} \end{bmatrix} = \mathbf{M}_p + \mathbf{M}_G + \begin{bmatrix} \left(I_{yy,p} - I_{zz,p}\right)\omega_{y,p}\omega_{z,p} \\ \left(I_{zz,p} - I_{xx,p}\right)\omega_{z,p}\omega_{x,p} \\ \left(I_{xx,p} - I_{yy,p}\right)\omega_{x,p}\omega_{y,p} \end{bmatrix}. \quad (22b)$$

Note that $\mathbf{M}_p = \sum_{i=1}^{N} \mathbf{m}_{\text{Muscle,i}}$, where $\mathbf{m}_{\text{Muscle,i}}$ is the moment of the tensegrity muscle force $-\mathbf{F}_{\text{Muscle,i}}$ about the center of gravity. Furthermore, $\mathbf{F}_G$ and $\mathbf{M}_G$ are the external forces and moments originating from wind-induced forces and/or manipulation forces applied by grippers O_1, O_2, and O_3.

4.4. Motion constraints

This paper assumes tensegrity muscles are sufficiently stiff that length of connecting tensegrity muscle i is almost constant at any time t. Let $L_{0,i} \in \mathbb{R}_+$ be the length of muscle i. Then,

$$i \in \mathcal{V},\ \forall t \geq t_0,\ \mathcal{C}_i = \left(x_i - x_{\zeta_i}\right)^2 + \left(y_i - y_{\zeta_i}\right)^2 + \left(z_{d,i} - z_{\zeta_i}\right)^2 \cong L_{0,i}.$$

Given x_i, y_i, x_{ζ_i}, y_{ζ_i}, and z_{ζ_i}, $z_{d,i}$ is obtained as follows:

$$z_{d,i} = z_{\zeta_i} + \sqrt{L_{0,i} - \left(x_{\zeta_i} - x_i\right)^2 + \left(y_{\zeta_i} - y_i\right)^2}. \quad (23)$$

By taking time derivatives of $\mathcal{C}_i$, $\dot{z}_{d,i} \cdots, z_{d,i}^{(\text{iv})}$ are assigned. In this paper, the z_i component of quadcopter i is updated by the following fourth-order and second-order dynamics:

Position control:

$$\frac{d^4 z_i}{dt^4} = \frac{d^4 z_{d,i}}{dt^4} + \sum_{j=1}^{4} \gamma_{j,i} \left(\frac{d^{4-j} z_{d,i}}{dt^{4-j}} - \frac{d^{4-j} z_i}{dt^{4-j}} \right) \quad (24a)$$

Force control:

$$\frac{d^2 z_i}{dt^2} = \frac{d^2 z_{d,i}}{dt^2} + \sum_{j=1}^{2} \gamma_{j,i} \left(\frac{d^{2-j} z_{d,i}}{dt^{2-j}} - \frac{d^{2-j} z_i}{dt^{2-j}} \right), \quad (24b)$$

where $\gamma_{1,i}$ through $\gamma_{4,i}$ are selected such that dynamics (24) is stable. Position control and force control will be discussed in Sections 5.1 and 5.2, respectively.

5. CALM control system

The dynamics of quadcopter i can be expressed in the following affine form:

$$\begin{cases} \dot{\mathcal{X}}_i = \mathbf{F}_i\left(\mathcal{X}_i\right) + G \begin{bmatrix} \mathbf{V}_i \\ u_{\psi,i} \end{bmatrix} + \mathbf{F}_{d,i} \\ \mathbf{r}_i = [x_i\ y_i\ z_i]^T \\ \mathcal{Y}_i = [x_i\ y_i]^T \end{cases}, \quad (25)$$

where $\mathcal{X}_i = [x_i\ \ y_i\ \ z_i\ \ v_{x,i}\ \ v_{y,i}\ \ v_{z,i}\ \ \bar{F}_{T,i}\ \ \phi_i\ \ \theta_i\ \ \psi_i\ \ \dot{\bar{F}}_{T,i}\ \ \dot{\phi}_i\ \ \dot{\theta}_i\ \ \dot{\psi}_i]^T \in \mathbb{R}^{14\times 1}$ is the control state, and $\mathbf{r}_i$ and $\mathcal{Y}_i$ denote the actual position and control output of quadcopter i, respectively. Moreover, $\mathbf{V}_i = [u_{T,i}\ u_{\phi,i}\ u_{\theta,i}]^T$, $G = [0_{4\times 10}\ I_4]^T$, $\mathbf{F}_{d,i} = [\mathbf{0}_{1\times 6}\ \ddot{\bar{\mathbf{F}}}^T_{\text{EXT},i}\ \mathbf{0}_{1\times 5}]^T$

$$\mathbf{F}_i = [v_{x,i}\ v_{y,i}\ v_{z,i}\ f_4\ f_5\ f_6\ \dot{\bar{F}}_{T,i}\ \dot{\phi}_i\ \dot{\theta}_i\ \dot{\psi}_i\ 0\ 0\ 0\ 0]^T$$

$$\begin{bmatrix} f_{4,i} \\ f_{5,i} \\ f_{6,i} \end{bmatrix} = \begin{bmatrix} 0 \\ 0 \\ -g \end{bmatrix} + \bar{F}_{T,i} \begin{bmatrix} C_{\phi_i} S_{\theta_i} C_{\psi_i} + S_{\phi_i} S_{\psi_i} \\ C_{\phi_i} S_{\theta_i} S_{\psi_i} - S_{\phi_i} C_{\psi_i} \\ C_{\phi_i} C_{\theta_i} \end{bmatrix} + \bar{\mathbf{F}}_{\text{EXT},i}.$$

Yaw control: In this paper, we assume that $u_{\psi,i} = \ddot{\psi}_{d,i} + k_{\dot{\psi}_i}\left(\dot{\psi}_{d,i} - \ddot{\psi}_i\right) + k_{\psi_i}\left(\dot{\psi}_{d,i} - \ddot{\psi}_i\right)$, where k_{ψ_i} and $k_{\dot{\psi}_i}$ are positive constants and $\psi_{d,i}$, $\dot{\psi}_{d,i}$, and $\ddot{\psi}_{d,i}$ are known. Therefore, ψ_i is updated by the following stable second order dynamics:

$$\left(\ddot{\psi}_i - \ddot{\psi}_{d,i}\right) + k_{\dot{\psi}_i}\left(\dot{\psi}_i - \dot{\psi}_{d,i}\right) + k_{\psi_i}\left(\psi_i - \psi_{d,i}\right) = 0. \quad (26)$$

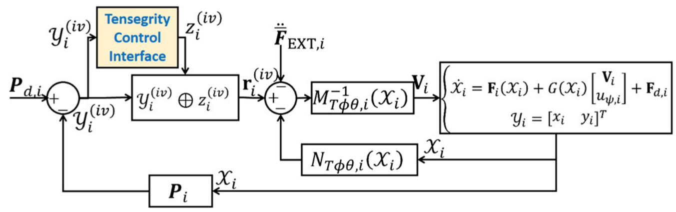

Fig. 4. Quadcopter i position controller block diagram.

The quadcopter i control system consists of three operation modes: (i) a closed-loop position control (PC), (ii) a closed-loop force control (FC), and (iii) an open-loop rigid body motion (RBM). Position control tracks a desired trajectory defined by a continuum deformation. In force control mode the MUS acts as stationary supports for the tensegrity muscles connected to grippers O_1, O_2, and O_3. In RBM mode, the thrust force exerted on quadcopter i remains constant.

5.1. Position control

Quadcopter i applies input–output (IO) feedback linearization control to track the desired trajectory $\mathbf{r}_{d,i}$. The controller block diagram is shown in Fig. 4.

The second time derivative of the Eq. (15) second row is:

$$\begin{bmatrix} x_i^{(\text{iv})} & y_i^{(\text{iv})} & z_i^{(\text{iv})} \end{bmatrix}^T = M_{T\phi\theta,i} \begin{bmatrix} u_{T,i} \\ u_{\phi,i} \\ u_{\psi,i} \end{bmatrix} + N_{T\phi\theta,i} + \ddot{\bar{\mathbf{F}}}_{\text{EXT},i}, \quad (27)$$

where

$$M_{T\phi\theta,i}\left(\phi_i, \theta_i, \psi_i\right) = \begin{bmatrix} \Lambda_{1,i} & \Lambda_{2,i} & \Lambda_{3,i} \end{bmatrix} \in \mathbb{R}^{3\times 3}, \quad (28a)$$

$$N_{T\phi\theta,i} = \dot{\Lambda}_{0,i} + \dot{\Lambda}_{1,i}\dot{\bar{F}}_{T,i} + \dot{\Lambda}_{2,i}\dot{\phi}_i + \dot{\Lambda}_{3,i}\dot{\theta}_{T,i} \in \mathbb{R}^{3\times 1}, \quad (28b)$$

$$\Lambda_{0,i} = \dot{\psi}_i \begin{bmatrix} -C_{\phi_i} S_{\theta_i} S_{\psi_i} + S_{\phi_i} C_{\psi_i} \\ C_{\phi_i} S_{\theta_i} C_{\psi_i} + S_{\phi_i} S_{\psi_i} \\ 0 \end{bmatrix}, \quad (28c)$$

$\Lambda_{1,i} = \Lambda_{1,i}(\phi_i, \theta_i, \psi_i)$, $\Lambda_{2,i} = \Lambda_{2,i}(\phi_i, \theta_i, \psi_i)$, and $\Lambda_{3,i} = \Lambda_{3,i}(\phi_i, \theta_i, \psi_i)$.

On the other hand,

$$\begin{bmatrix} x_i^{(\text{iv})} & y_i^{(\text{iv})} & z_i^{(\text{iv})} \end{bmatrix}^T = \mathbf{U}_i. \quad (29)$$

Defining $\mathbf{P}_i = \sum_{j=1}^{4} \gamma_{j,i} \frac{d^{4-j}\mathcal{Y}_i}{dt^{4-j}}$ and $\mathbf{P}_{d,i}^{\mu_i} = \sum_{j=0}^{\mu_i} \gamma_{4-j,i} \frac{d^j \mathcal{Y}_{d,i}}{dt^j}$, we choose

$$\mathbf{U}_i = \begin{bmatrix} \mathbf{P}_{d,i}^{\mu_i} - \mathbf{P}_i \\ z_i^{(\text{iv})} \end{bmatrix}. \quad (30)$$

Notice that $\mu_i = 3$ if $i \in \mathcal{V}_F$; otherwise, $\mu_i = 4$ and $\gamma_{0,i} = 1$. Also, $z_i^{(\text{iv})}$ is updated by Eq. (24a). Furthermore, $\gamma_{1,i}, \gamma_{2,i}, \gamma_{3,i}, \gamma_{4,i} > 0$ are chosen such that the MUS collective dynamics is stable. Note that MUS collective dynamics stability is discussed in Section 6. By equating the right-hand sides of Eqs. (27) and (29), the control $\mathbf{V}_i = [u_{T,i}\ u_{\phi,i}\ u_{\theta,i}]^T$ is obtained as follows:

$$\mathbf{V}_i = M_{T\phi\theta,i}^{-1}\left(\mathbf{U}_i - N_{T\phi\theta,i} - \ddot{\bar{F}}_{\text{EXT},i}\right). \quad (31)$$

5.2. Force control

For force control mode, force $\bar{\mathbf{F}}_{\text{EXT},i} = \bar{\mathbf{F}}_{\text{Muscle},i}$ and $\mathbf{r}_{d,i}$ are the reference inputs. It is assumed that quadcopter i's force sensor can accurately measure the force $\bar{\mathbf{F}}_{\text{EXT},i}$ exerted by tensegrity muscle i.

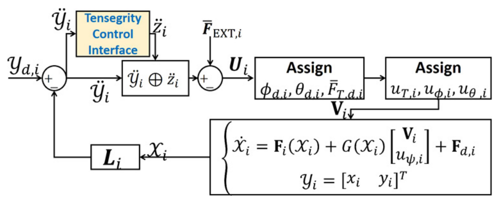

Fig. 5. Quadcopter i force controller block diagram.

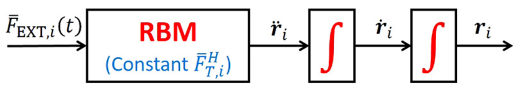

Fig. 6. Quadcopter i rigid body motion (RBM) block diagram.

Furthermore, quadcopter i's desired position, denoted by $\mathbf{r}_{d,i}$, is known and constant. Let

$$\mathbf{L}_i = \gamma_{1,i}\frac{\mathrm{d}\mathcal{Y}_i}{\mathrm{d}t} + \gamma_{2,i}\mathcal{Y}_i \tag{32}$$

where $\gamma_{1,i}, \gamma_{2,i} > 0$. $\mathcal{Y}_i$ asymptotically converges to zero, if $\mathcal{Y}_i$ is updated by the following second order dynamics:

$$\frac{\mathrm{d}^2\mathcal{Y}_i}{\mathrm{d}t^2} = \mathcal{Y}_{d,i} - \mathbf{L}_i. \tag{33}$$

For force control,

$$\mathbf{U}_i = \begin{bmatrix} u_{i,1} \\ u_{i,2} \\ u_{i,3} \end{bmatrix} = \begin{bmatrix} \mathcal{Y}_{d,i} - \mathbf{L}_i \\ \ddot{z}_i \end{bmatrix} + \begin{bmatrix} 0 \\ 0 \\ g \end{bmatrix} - \bar{\mathbf{F}}_{\text{EXT},i}, \tag{34}$$

where $\ddot{z}_i$ is updated by Eq. (24b). Given $\mathbf{U}_i$, desired thrust per mass $\bar{F}_{T,d,i}$ and Euler angles $\phi_{d,i}$ and $\theta_{d,i}$ are obtained as:

$$\bar{F}_{T,d,i} = \|\mathbf{U}_i\|, \tag{35a}$$

$$\phi_{d,i} = -\sin^{-1}\left(\left(u_{1,i}S_{\psi_i} - u_{2,i}C_{\psi_i}\right)/\|\mathbf{U}_i\|\right), \tag{35b}$$

$$\theta_{d,i} = \tan^{-1}\left(\left(u_{1,i}C_{\psi_i} + u_{2,i}S_{\psi_i}\right)/u_{3,i}\right). \tag{35c}$$

Quadcopter i input $\mathbf{V}_i = [u_{T,i} \; u_{\phi,i} \; u_{\theta,i}]^T$ is chosen as:

$$\begin{bmatrix} u_{T,i} \\ u_{\theta,i} \\ u_{\psi,i} \end{bmatrix} = \begin{bmatrix} -k_{\dot{T}_i}\dot{\bar{F}}_{T,i} + k_{T_i}\left(\bar{F}_{T,d,i} - \bar{F}_{T,i}\right) \\ -k_{\dot{\phi}_i}\dot{\phi}_i + k_{\phi_i}\left(\phi_{d,i} - \phi_i\right) \\ -k_{\dot{\theta}_i}\dot{\theta}_i + k_{\theta_i}\left(\theta_{d,i} - \theta_i\right) \end{bmatrix}, \tag{36}$$

where $k_{T_i}, k_{\dot{T}_i}, k_{\phi_i}, k_{\dot{\phi}_i}, k_{\theta_i}, k_{\dot{\theta}_i} > 0$. The quadcopter i force controller is shown in Fig. 5.

5.3. Rigid-body motion (RBM)

In rigid body motion mode the thrust force per mass exerted on quadcopter i, denoted by $\bar{F}^H_{T,i}$, is constant. Let $\bar{\mathbf{F}}^H_{\text{EXT},i} = \bar{\mathbf{F}}^H_{\text{Muscle},i}$ is the force per mass exerted by quadcopter i at the static equilibrium (hovering) condition. At the hovering condition $\dot{\mathbf{v}}_i$ vanishes (see the second row of Eq. (15)), and the hovering thrust force per mass $\bar{F}^H_{T,i}$ is obtained as follows:

$$\bar{F}^H_{T,i} = \|g\hat{\mathbf{e}}_3 + \bar{\mathbf{F}}^H_{\text{EXT},i}\|. \tag{37}$$

In the RBM mode, the acceleration of quadcopter i is obtained using Newton's second law:

$$\ddot{\mathbf{r}}_i = \bar{F}^H_{T,i} = \bar{\mathbf{F}}_{\text{EXT},i} + \bar{F}^H_{T,i}\mathbf{k}_{b,i} - g\hat{\mathbf{e}}_3. \tag{38}$$

The RBM dynamics mode is illustrated in Fig. 6.

6. MUS as a moving support

In the transportation task, each quadcopter acts as a moving support and applies position control from Section 5.1 to track desired trajectory. When quadcopters act as moving supports, MUS desired coordination is decomposed into two modes: (i) MUS continuum deformation and (ii) Constrained motion along the z axis. Note that MUS coordination in the X–Y plane is free. The z component of quadcopter i coordination is determined by the motion constraints from Section 4.4.

6.1. Agent coordination

MUS continuum deformation in the X–Y plane can be defined based on the trajectories chosen by three leaders in Section 6.2. Followers acquire a desired continuum deformation through local communication. Let local desired position $\mathcal{Y}_{d,i} = \sum_{j\in\mathcal{N}_i} w_{i,j}\mathcal{Y}_j$ ($i \in \mathcal{V}_F$) be substituted in Eqs. (29) and (30) and followers communication weights satisfy Eq. (12).

Given $\gamma_{j,i}$, ($j = 1, 2, 3, 4$, $i \in \mathcal{V}$), we define the following positive-definite diagonal gain matrices:

$$G_{j,L} = \mathrm{diag}\left(\gamma_{1,j}, \gamma_{2,j}, \gamma_{3,j}\right) \in \mathbb{R}^{3\times 3}, \tag{39a}$$

$$G_{j,F} = \mathrm{diag}\left(\gamma_{4,j}, \cdots, \gamma_{N,j}\right) \in \mathbb{R}^{(N-3)\times(N-3)}. \tag{39b}$$

Before obtaining MUS coordination dynamics, we define the following vectors: $\mathbf{Z}^T_{L,q} = [q_1 \; q_2 \; q_3]$, $\mathbf{Z}^T_{F,q} = [q_4 \; \cdots \; q_N]$, $\mathbf{Z}^T_{L,q,HT} = [q_{1,HT} \; q_{2,HT} \; q_{3,HT}]$, and $\mathbf{Z}^T_{F,q,HT} = [q_{4,HT} \; \cdots \; q_{N,HT}]$ ($q = x, y$). Note that $\mathbf{Z}_{F,q,HT} = W_L\mathbf{Z}_{L,q,HT}$ assigns component q of the follower quadcopter global desired positions given by continuum deformation (Eqs. (10) and (14)).

$$\mathbf{U}_{\text{MUS},q} = \sum_{j=0}^{4} G_{j,L}\frac{\mathrm{d}^{4-j}\mathbf{Z}_{L,q,HT}}{\mathrm{d}t^{4-j}} \tag{40}$$

as the reference input of the coordination dynamics. If the position of every quadcopter is updated according to the dynamics in Eqs. (29) and (30), then MUS collective dynamics becomes

$$\frac{\mathrm{d}^4\mathbf{Z}_{L,q}}{\mathrm{d}t^4} = \frac{\mathrm{d}^4\mathbf{Z}_{L,q,HT}}{\mathrm{d}t^4} + \sum_{j=1}^{4} G_{j,L}\frac{\mathrm{d}^{4-j}\left(\mathbf{Z}_{L,q,HT} - \mathbf{Z}_{L,q}\right)}{\mathrm{d}t^{4-j}} \tag{41a}$$

$$\frac{\mathrm{d}^4\mathbf{Z}_{F,q}}{\mathrm{d}t^4} = \sum_{j=1}^{4} G_{j,F}A\frac{\mathrm{d}^{4-j}\mathbf{Z}_{F,q}}{\mathrm{d}t^{4-j}} + \sum_{j=1}^{4} G_{j,F}B\frac{\mathrm{d}^{4-j}\mathbf{Z}_{L,q}}{\mathrm{d}t^{4-j}}. \tag{42}$$

Theorem 1. *Define $\mathbf{E}_{L,q} = \mathbf{Z}_{L,q} - \mathbf{Z}_{L,q,HT}$ and $\mathbf{E}_{F,q} = \mathbf{Z}_{F,q} - \mathbf{Z}_{F,q,HT}$ as the error signals specifying deviation of leader and follower quadcopters from global desired positions given by the continuum deformation. The error signals $\mathbf{E}_{L,q}$ and $\mathbf{E}_{F,q}$ are updated by the following fourth order dynamics:*

$$\frac{\mathrm{d}^4\mathbf{E}_{L,q}}{\mathrm{d}t^4} = \sum_{j=1}^{4} G_{j,L}\frac{\mathrm{d}^{4-j}\left(\mathbf{E}_{L,q}\right)}{\mathrm{d}t^{4-j}} \tag{43a}$$

$$\frac{\mathrm{d}^4\mathbf{E}_{F,q}}{\mathrm{d}t^4} = \sum_{j=1}^{4} G_{j,F}\left(A\frac{\mathrm{d}^{4-j}\mathbf{E}_{F,q}}{\mathrm{d}t^{4-j}} + B\frac{\mathrm{d}^{4-j}\mathbf{E}_{L,q}}{\mathrm{d}t^{4-j}}\right) - W_L\frac{\mathrm{d}^4\mathbf{Z}_{L,q,HT}}{\mathrm{d}t^4}. \tag{43b}$$

Proof. By subtracting $\frac{\mathrm{d}^4\mathbf{Z}_{L,q,HT}}{\mathrm{d}t^4}$ from both sides of Eq. (41a), Eq. (41a) can be rewritten as Eq. (43a) and (42) becomes

$$\frac{\mathrm{d}^4\mathbf{Z}_{F,q}}{\mathrm{d}t^4}=\sum_{j=1}^{4}G_{j,F}\left(A\frac{\mathrm{d}^{4-j}\mathbf{Z}_{F,q}}{\mathrm{d}t^{4-j}}+B\frac{\mathrm{d}^{4-j}\mathbf{Z}_{L,q,HT}}{\mathrm{d}t^{4-j}}+B\frac{\mathrm{d}^{4-j}\mathbf{E}_{L,q}}{\mathrm{d}t^{4-j}}\right). \tag{44}$$

Substituting $B=-AW_L$, Eq. (44) can be rewritten as follows:

$$\frac{\mathrm{d}^4\mathbf{Z}_{F,q}}{\mathrm{d}t^4}=\sum_{j=1}^{4}G_{j,F}A\frac{\mathrm{d}^{4-j}\mathbf{E}_{F,q}}{\mathrm{d}t^{4-j}}+\sum_{j=1}^{4}G_{j,F}B\frac{\mathrm{d}^{4-j}\mathbf{E}_{L,q}}{\mathrm{d}t^{4-j}}. \tag{45}$$

By subtracting $\frac{\mathrm{d}^4\mathbf{Z}_{F,q,HT}}{\mathrm{d}t^4}=W_L\frac{\mathrm{d}^4\mathbf{Z}_{L,q,HT}}{\mathrm{d}t^4}$ from both sides of Eq. (45), $\mathbf{E}_{F,q}$ is updated by Eq. (43b). □

Remark. In collective dynamics characteristic equation, $\left|s^4 I_{N-3}-\sum_{j=0}^{3}s^jG_{4-j,F}A\right|=0$, roots are all placed in the left-hand side of the s-plane.

Theorem 2. *Let d_s be the distance between the closest quadcopters at initial time t_0 and d_b be the closest distance of a quadcopter from the sides of the leading triangle forms by three leaders. Suppose $\lambda_{\mathrm{CD,min}}>0$ assigns a lower-limit for eigenvalues of the pure deformation matrix U_{CD}, e.g $\lambda_{\mathrm{CD,min}}\le\lambda_1(U_{\mathrm{CD}})\le\lambda_1(U_{\mathrm{CD}})$. Assume each quadcopter is enclosed by a ball with radius ϵ. Define*

$$\delta_{\max}=\left\{\frac{1}{2}(d_s-2\epsilon),d_b-\epsilon\right\}. \tag{46}$$

Inter-agent collision in a MUS continuum deformation is avoided, if the following inequalities are both satisfied:

$$\forall i\in\mathcal{V},\qquad \|\mathcal{Y}_i-\mathcal{Y}_{i,HT}\|\le\delta \tag{47a}$$

$$\frac{\delta+\epsilon}{\delta_{\max}+\epsilon}\le\lambda_{\mathrm{CD,min}}. \tag{47b}$$

Proof. See the proof in [57]. □

6.2. Leaders' evolution during TT

The leader quadcopters' coordinated global desired trajectory is assigned by solving a constrained optimal control problem. Let x and y components of the leaders' desired positions be updated by the following second order dynamics:

$$i\in\mathcal{V}_L,\ q=x,y,\qquad \ddot{q}_{i,HT}=u_{q,i,HT} \tag{48}$$

where $u_{x,i,HT}$ and $u_{y,i,HT}$ are inputs. The area of the leading triangle must remain constant at any time t; therefore, desired leaders' trajectories must satisfy the following constraint:

$$C_L=\begin{vmatrix}x_{1,HT} & x_{2,HT} & x_{3,HT}\\ y_{1,HT} & y_{2,HT} & y_{3,HT}\\ 1 & 1 & 1\end{vmatrix}-2a_0=0, \tag{49}$$

where a_0 is the area of the leading triangle at initial time t_0. Without loss of generality, we consider

$$J=\int_0^{T_{\mathrm{mission}}}\sum_{i=1}^{3}\left(u_{x,i,HT}^2+u_{y,i,HT}^2\right)\mathrm{d}t \tag{50}$$

as the optimal control cost, where T_{mission} is fixed. The solution of the above optimal control problem is presented in Appendix A and [60].

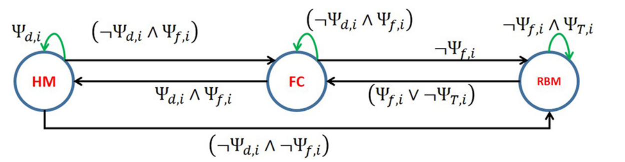

Fig. 7. HFC hybrid dynamic model.

7. An MUS as stationary supports

The MUS is commanded to remain stationary to simulate a fixed-base manipulation platform when grippers carry multi-degree-of-freedom manipulation arms. To stabilize the MUS, we propose a hybrid force control (HFC) model with the following three operation modes:

1. HM: quadcopter i "Hover Mode" condition is active.
2. RBM: quadcopter i is at the "Rigid Body Motion" mode.
3. FC: quadcopter i is at the "Force Control" Mode.

Let quadcopter i's desired XY position, denoted by $\mathcal{Y}_{d,i}=[x_{d,}\ \ y_{d,i}]^T$, be constant and let the threshold distance d_{Thresh}, time threshold T_{Thresh}, threshold force magnitudes f_{Thresh}, threshold force rate $\dot{f}_{\mathrm{Thresh}}$ all be known. We define the following atomic propositions to construct transitions between the HFC discrete nodes:

$$i=1,\cdots,N,\qquad \Psi_{d,i}:=\|\mathcal{Y}_i-\mathcal{Y}_{d,i}\|-d_{\mathrm{Thresh}}\le 0,$$
$$i=1,\cdots,N,\qquad \Psi_{f,i}:=\|\bar{\mathbf{F}}_{\mathrm{EXT},i}\|-f_{\mathrm{Thresh}}\le 0,$$
$$i=1,\cdots,N,\qquad \Psi_{T,i}:=t-t_{\mathrm{RBM}}-T_{\mathrm{Thresh}}\le 0.$$

Note that t_{RBM} and t denote the time system entered the RBM and the current time. The HFC hybrid dynamic model is shown in Fig. 7. Note the $\neg$, $\wedge$, and $\vee$ are logical operators implying "negation", "conjunction", and "disjunction", respectively.

HFC interpretation: Functionality of the HFC is described by the following statements:

- Quadcopter i is at the hovering condition until $\Psi_{d,i}=\|\mathcal{Y}_i-\mathcal{Y}_{d,i}\|-d_{\mathrm{Thresh}}\le 0$ is violated.
- If $\|\mathcal{Y}_i-\mathcal{Y}_{d,i}\|-d_{\mathrm{Thresh}}\le 0$ is violated but $\Psi_{f,i}=\|\bar{\mathbf{F}}_{\mathrm{EXT},i}\|-f_{\mathrm{Thresh}}\le 0$ is satisfied, "FC" mode is activated.
- Quadcopter i activates the "RBM", if both $\Psi_{d,i}=\|\mathcal{Y}_i-\mathcal{Y}_{d,i}\|-d_{\mathrm{Thresh}}\le 0$ and $\Psi_{f,i}=\|\bar{\mathbf{F}}_{\mathrm{EXT},i}\|-f_{\mathrm{Thresh}}\le 0$ are violated.
- Quadcopter i leaves the "RBM" and activates the "FC" mode, if $\Psi_{f,i}=\|\bar{\mathbf{F}}_{\mathrm{EXT},i}\|-f_{\mathrm{Thresh}}\le 0$ is violated or $\Psi_{T,i}:=t-t_0-T_{\mathrm{Thresh}}\le 0$ is not satisfied.
- Quadcopter i leaves the "FC" modes returns to mode "HM", if $\Psi_{d,i}=\|\mathcal{Y}_i-\mathcal{Y}_{d,i}\|-d_{\mathrm{Thresh}}\le 0$ is satisfied.

8. MUS-payload system stability

Tensegrity muscles can carry both tension and compression forces, and tensegrity arms are connected to the payload at three non-aligned points O_1, O_2, and O_3. Therefore, the payload is almost rigid with respect to the MUS and rotation angles ϕ_p and θ_p are small ($\phi_p\cong\theta_p\cong 0$). Let

$$i=1,\cdots,N,\qquad \mathbf{r}_{\zeta_i}=\mathbf{r}_p+\mathbf{d}_{\zeta_i}, \tag{51a}$$

$$i=1,\cdots,N,\qquad \mathbf{d}_{\zeta_i}=d_{x,\zeta_i}\hat{\mathbf{e}}_1+d_{y,\zeta_i}\hat{\mathbf{e}}_2+d_{z,\zeta_i}\hat{\mathbf{e}}_3 =\begin{bmatrix}d_{x,\zeta_i} & d_{y,\zeta_i} & d_{z,\zeta_i}\end{bmatrix}^T, \tag{51b}$$

where ζ_i was previously defined in Section 4.2. Eq. (51) implies that

$$i=1,\cdots,N, \qquad x_{\zeta_i}=x_p+d_{x,\zeta_i} \tag{52a}$$

$$i=1,\cdots,N, \qquad y_{\zeta_i}=y_p+d_{y,\zeta_i}. \tag{52b}$$

Assuming $\dot{\psi}_p$ is small, then, $\dot{\mathbf{d}}_{\zeta_i}\cong\mathbf{0}$, $\dot{\mathbf{d}}_{x,\zeta_i}\cong 0$, $\dot{\mathbf{d}}_{y,\zeta_i}=0$, $\dot{\mathbf{d}}_{z,\zeta_i}=0$, $\ddot{\mathbf{d}}_{\zeta_i}\cong\mathbf{0}$, $\ddot{\mathbf{d}}_{x,\zeta_i}\cong 0$, $\ddot{\mathbf{d}}_{y,\zeta_i}=0$, and $\ddot{\mathbf{d}}_{z,\zeta_i}=0$ $(i=1,\cdots,N)$. Therefore,

$$q=x,y,z, \qquad \dot{q}_p=\dot{q}_{O_1}=\dot{q}_{O_2}=\dot{q}_{O_3}$$
$$\ddot{q}_p=\ddot{q}_{O_1}=\ddot{q}_{O_2}=\ddot{q}_{O_3}$$

8.1. Position control mode[1]

For the position control mode, quadcopter $i\in\mathcal{V}$ is modeled by a feedback linearizable dynamics and position of quadcopter i is updated by the fourth-order dynamics given in (29) and (30). Define

$$q=x,y,z,$$
$$\mathbf{X}^{\mathrm{PC}}_{\mathrm{SYS},q}=[q_1\ \cdots\ q_N\ \dot{q}_1\ \cdots\ \dot{q}_N\ \ddot{q}_1\ \cdots\ \ddot{q}_N\ \dddot{q}_1\ \cdots\ \dddot{q}_N]^T\in\mathbb{R}^{4N\times 1}, \tag{53a}$$

$$\mathbf{X}_{\mathrm{SYS},p}=\begin{bmatrix}x_p & y_p & z_p & \dot{x}_p & \dot{y}_p & \dot{z}_p\end{bmatrix}\in\mathbb{R}^{6\times 1}, \tag{53b}$$

$$j=1,\cdots,4, \qquad G_j=\mathrm{diag}\left(\gamma_{1,j},\gamma_{2,j},\cdots,\gamma_{N,j}\right)\in\mathbb{R}^{N\times N}, \tag{53c}$$

$$\mathbf{\Gamma}=\begin{bmatrix}-\mathbf{I}_3 & \mathbf{0}_{3\times(N-3)}\\ B & A\end{bmatrix}\in\mathbb{R}^{N\times N}, \tag{53d}$$

$$\mathbf{\Omega}^{\mathrm{PC}}_{xy}=\begin{bmatrix}\mathbf{0}_N & \mathbf{I}_N & \mathbf{0}_N & \mathbf{0}_N\\ \mathbf{0}_N & \mathbf{0}_N & \mathbf{I}_N & \mathbf{0}_N\\ \mathbf{0}_N & \mathbf{0}_N & \mathbf{0}_N & \mathbf{I}_N\\ G_4\mathbf{\Gamma} & G_3\mathbf{\Gamma} & G_2\mathbf{\Gamma} & G_1\mathbf{\Gamma}\end{bmatrix}\in\mathbb{R}^{4N\times 4N}, \tag{53e}$$

$$\mathbf{\Omega}^{\mathrm{PC}}_{z}=\begin{bmatrix}\mathbf{0}_N & \mathbf{I}_N & \mathbf{0}_N & \mathbf{0}_N\\ \mathbf{0}_N & \mathbf{0}_N & \mathbf{I}_N & \mathbf{0}_N\\ \mathbf{0}_N & \mathbf{0}_N & \mathbf{0}_N & \mathbf{I}_N\\ -G_4 & -G_3 & -G_2 & -G_1\end{bmatrix}\in\mathbb{R}^{4N\times 4N}, \tag{53f}$$

$$\mathbf{\Omega}_{p,p}=\begin{bmatrix}-\frac{1}{m_p}\sum_{i=1}^N k_i\mathbf{I}_3 & \mathbf{0}_3\\ \mathbf{0}_3 & -\frac{1}{m_p}\sum_{i=1}^N c_i\mathbf{0}_3\end{bmatrix}\in\mathbb{R}^{6\times 6}, \tag{53g}$$

where $A\in\mathbb{R}^{(N-3)\times(N-3)}$ and $B\in\mathbb{R}^{(N-3)\times 3}$ were previously defined in (13), $\mathbf{I}_N\in\mathbb{R}^{N\times N}$ and $\mathbf{I}_3\in\mathbb{R}^{3\times 3}$ are the identity matrices and $\mathbf{0}_{3\times(N-3)}\in\mathbb{R}^{3\times(N-3)}$ and $\mathbf{0}_N$ are zero-entry matrices. Furthermore, we define

$$\mathbf{\Omega}^{\mathrm{PC}}_{p,x}=\begin{bmatrix}\mathbf{K}_{p,xyz} & \mathbf{0}_{1\times N} & \mathbf{0}_{1\times 2N}\\ \mathbf{0}_{2\times N} & \mathbf{0}_{2\times N} & \mathbf{0}_{1\times 2N}\\ \mathbf{0}_{1\times N} & \mathbf{C}_{p,xyz} & \mathbf{0}_{1\times 2N}\\ \mathbf{0}_{2\times N} & \mathbf{0}_{2\times N} & \mathbf{0}_{1\times 2N}\end{bmatrix}\in\mathbb{R}^{6\times 4N}, \tag{54a}$$

$$\mathbf{\Omega}^{\mathrm{PC}}_{p,y}=\begin{bmatrix}\mathbf{0}_{1\times N} & \mathbf{0}_{1\times N} & \mathbf{0}_{1\times 2N}\\ \mathbf{K}_{p,xyz} & \mathbf{0}_{1\times N} & \mathbf{0}_{1\times 2N}\\ \mathbf{0}_{2\times N} & \mathbf{0}_{2\times N} & \mathbf{0}_{2\times 2N}\\ \mathbf{0}_{1\times N} & \mathbf{C}_{p,xyz} & \mathbf{0}_{1\times 2N}\\ \mathbf{0}_{1\times N} & \mathbf{0}_{1\times N} & \mathbf{0}_{1\times 2N}\end{bmatrix}\in\mathbb{R}^{6\times 4N}, \tag{54b}$$

$$\mathbf{\Omega}^{\mathrm{PC}}_{p,z}=\begin{bmatrix}\mathbf{0}_{2\times N} & \mathbf{0}_{2\times N} & \mathbf{0}_{1\times 2N}\\ \mathbf{K}_{p,xyz} & \mathbf{0}_{1\times N} & \mathbf{0}_{1\times 2N}\\ \mathbf{0}_{2\times N} & \mathbf{0}_{2\times N} & \mathbf{0}_{1\times 2N}\\ \mathbf{0}_{1\times N} & \mathbf{C}_{p,xyz} & \mathbf{0}_{1\times 2N}\end{bmatrix}\in\mathbb{R}^{6\times 4N}, \tag{54c}$$

where

$$\mathbf{K}_{p,xyz}=\frac{1}{m_p}\begin{bmatrix}k_1 & k_2 & \cdots & k_N\end{bmatrix}\in\mathbb{R}^{1\times N}, \tag{55a}$$

$$\mathbf{C}_{p,xyz}=\frac{1}{m_p}\begin{bmatrix}c_1 & c_2 & \cdots & c_N\end{bmatrix}\in\mathbb{R}^{1\times N}, \tag{55b}$$

$\mathbf{0}_{1\times N}\in\mathbb{R}^{1\times N}$, $\mathbf{0}_{1\times 2N}\in\mathbb{R}^{1\times 2N}$, $\mathbf{0}_{2\times N}\in\mathbb{R}^{2\times N}$, and $\mathbf{0}_{2\times 2N}\in\mathbb{R}^{2\times 2N}$ are the zero-entry matrices, and k_i and c_i denote the stiffness and damping of tensegrity muscle i, respectively. The MUS-payload dynamics is given by

$$\dot{\mathbf{X}}^{\mathrm{PC}}_{\mathrm{SYS}}=\mathbf{A}^{\mathrm{PC}}_{\mathrm{SYS}}\mathbf{X}^{\mathrm{PC}}_{\mathrm{SYS}}+\begin{bmatrix}\mathbf{B}^{\mathrm{PC}}_{\mathrm{SYS},xy} & \mathbf{0}_{4N\times 3} & \mathbf{0}_{4N\times N}\\ \mathbf{0}_{4N\times 3} & \mathbf{B}^{\mathrm{PC}}_{\mathrm{SYS},xy} & \mathbf{0}_{4N\times N}\\ \mathbf{0}_{4N\times 3} & \mathbf{0}_{4N\times 3} & \mathbf{B}^{\mathrm{PC}}_{\mathrm{SYS},z}\\ \mathbf{0}_{6\times 3} & \mathbf{0}_{6\times 3} & \mathbf{0}_{6\times N}\end{bmatrix}\mathbf{U}^{\mathrm{PC}}_{\mathrm{SYS}}+\mathbf{f}^{\mathrm{PC}}_{\mathrm{SYS}}, \tag{56}$$

where

$$\mathbf{X}^{\mathrm{PC}}_{\mathrm{SYS}}=\left[\left(\mathbf{X}^{\mathrm{PC}}_{\mathrm{SYS},x}\right)^T \quad \left(\mathbf{X}^{\mathrm{PC}}_{\mathrm{SYS},y}\right)^T \quad \left(\mathbf{X}^{\mathrm{PC}}_{\mathrm{SYS},z}\right)^T \quad \left(\mathbf{X}_{\mathrm{SYS},p}\right)^T\right]^T \in\mathbb{R}^{(12N+6)\times 1}, \tag{57a}$$

$$\mathbf{A}^{\mathrm{PC}}_{\mathrm{SYS}}=\begin{bmatrix}\mathbf{\Omega}^{\mathrm{PC}}_{xy} & \mathbf{0}_{4N} & \mathbf{0}_{4N} & \mathbf{0}_{4N\times 6}\\ \mathbf{0}_{4N} & \mathbf{\Omega}^{\mathrm{PC}}_{xy} & \mathbf{0}_{4N} & \mathbf{0}_{4N\times 6}\\ \mathbf{0}_{4N} & \mathbf{0}_{4N} & \mathbf{\Omega}^{\mathrm{PC}}_{z} & \mathbf{0}_{4N\times 6}\\ \mathbf{\Omega}^{\mathrm{PC}}_{p,x} & \mathbf{\Omega}^{\mathrm{PC}}_{p,y} & \mathbf{\Omega}^{\mathrm{PC}}_{p,z} & \mathbf{\Omega}^{\mathrm{PC}}_{p,p}\end{bmatrix}\in\mathbb{R}^{(12N+6)\times(12N+6)}, \tag{57b}$$

$$\mathbf{B}^{\mathrm{PC}}_{\mathrm{SYS},xy}=\begin{bmatrix}\mathbf{0}_{3\times 3N} & \mathbf{I}_3 & \mathbf{0}_{3\times(N-3)}\end{bmatrix}^T\in\mathbb{R}^{4N\times 3}, \tag{57c}$$

$$\mathbf{B}^{\mathrm{PC}}_{\mathrm{SYS},z}=\begin{bmatrix}\mathbf{0}_{N\times 3N} & \mathbf{I}_N\end{bmatrix}^T\in\mathbb{R}^{4N\times N}, \tag{57d}$$

$$\mathbf{f}^{\mathrm{PC}}_{\mathrm{SYS}}=\begin{bmatrix}\mathbf{0}_{1\times(12N+5)} & -g\end{bmatrix}^T+\begin{bmatrix}\mathbf{0}_{1\times(12N+3)} & -\frac{1}{m_p}\sum_{i=1}^N k_{\zeta_i}\mathbf{d}^T_{\zeta_i}\end{bmatrix}^T. \tag{57e}$$

Defining

$$\mathbf{U}^{\mathrm{PC}}_{\mathrm{MUS},z}=\begin{bmatrix}\frac{\mathrm{d}^4 z_{d,1}}{\mathrm{d}t^4} & \cdots & \frac{\mathrm{d}^4 z_{d,N}}{\mathrm{d}t^4}\end{bmatrix}^T+\sum_{j=1}^4 G_j\begin{bmatrix}\frac{\mathrm{d}^{4-j} z_{d,1}}{\mathrm{d}t^{4-j}} & \cdots & \frac{\mathrm{d}^{4-j} z_{d,N}}{\mathrm{d}t^{4-j}}\end{bmatrix}^T,$$

$\mathbf{U}^{\mathrm{PC}}_{\mathrm{SYS}}\in\mathbb{R}^{(N+6)\times 1}$ is given by

$$\mathbf{U}^{\mathrm{PC}}_{\mathrm{SYS}}=\left[\left(\mathbf{U}^{\mathrm{PC}}_{\mathrm{MUS},x}\right)^T \quad \left(\mathbf{U}^{\mathrm{PC}}_{\mathrm{MUS},y}\right)^T \quad \left(\mathbf{U}^{\mathrm{PC}}_{\mathrm{MUS},z}\right)^T\right]^T, \tag{58}$$

where $\mathbf{U}^{\mathrm{PC}}_{\mathrm{MUS},x}=\mathbf{U}_{\mathrm{MUS},x}$ and $\mathbf{U}^{\mathrm{PC}}_{\mathrm{MUS},y}=\mathbf{U}_{\mathrm{MUS},y}$ were previously defined in Eq. (40).

Remark. Matrix $\mathbf{\Omega}_{p,p}$ and $\mathbf{\Omega}_z$ are Hurwitz. A is also Hurwitz, so $\mathbf{\Gamma}$ and $\mathbf{\Omega}_{xy}$ are Hurwitz as well. Matrix $\mathbf{A}_{\mathrm{SYS}}$ is Hurwitz because all block-diagonal matrices are Hurwitz. Consequently, the MUS-payload dynamics, given by Eq. (56), is stable.

8.2. Force control mode[2]

To analyze MUS-Payload stability in a force control task, UAVs are modeled as double integrators. Define

$$q=x,y,z, \qquad \mathbf{X}^{\mathrm{FC}}_{\mathrm{SYS},q}=[q_1\ \cdots\ q_N\ \dot{q}_1\ \cdots\ \dot{q}_N]^T\in\mathbb{R}^{2N\times 1}, \tag{59a}$$

$$\mathbf{\Omega}^{\mathrm{FC}}_{xy}=\begin{bmatrix}\mathbf{0}_N & \mathbf{I}_N\\ G_2\mathbf{\Gamma} & G_1\mathbf{\Gamma}\end{bmatrix}\in\mathbb{R}^{2N\times 2N}, \tag{59b}$$

[1] The superscript PC refers to "Position Control".

[2] The superscript FC is referred to "Force Control".

$$\mathbf{\Omega}_z^{FC} = \begin{bmatrix} \mathbf{0}_N & \mathbf{I}_N \\ -G_2 & -G_1 \end{bmatrix} \in \mathbb{R}^{2N\times 2N}, \tag{59c}$$

$$\mathbf{\Omega}_{p,x}^{FC} = \begin{bmatrix} \mathbf{K}_{p,xyz} & \mathbf{0}_{1\times N} \\ \mathbf{0}_{2\times N} & \mathbf{0}_{2\times N} \\ \mathbf{0}_{1\times N} & \mathbf{C}_{p,xyz} \\ \mathbf{0}_{2\times N} & \mathbf{0}_{2\times N} \end{bmatrix} \in \mathbb{R}^{6\times 2N}, \tag{59d}$$

$$\mathbf{\Omega}_{p,y}^{FC} = \begin{bmatrix} \mathbf{0}_{1\times N} & \mathbf{0}_{1\times N} \\ \mathbf{K}_{p,xyz} & \mathbf{0}_{1\times N} \\ \mathbf{0}_{2\times N} & \mathbf{0}_{2\times N} \\ \mathbf{0}_{1\times N} & \mathbf{C}_{p,xyz} \\ \mathbf{0}_{1\times N} & \mathbf{0}_{1\times N} \end{bmatrix} \in \mathbb{R}^{6\times 2N}, \tag{59e}$$

$$\mathbf{\Omega}_{p,z}^{FC} = \begin{bmatrix} \mathbf{0}_{2\times N} & \mathbf{0}_{2\times N} \\ \mathbf{K}_{p,xyz} & \mathbf{0}_{1\times N} \\ \mathbf{0}_{2\times N} & \mathbf{0}_{2\times N} \\ \mathbf{0}_{1\times N} & \mathbf{C}_{p,xyz} \end{bmatrix} \in \mathbb{R}^{6\times 2N}. \tag{59f}$$

Note that $\Gamma \in \mathbb{R}^{N\times N}$, $\mathbf{K}_{p,xyz} \in \mathbb{R}^{1\times N}$, $\mathbf{C}_{p,xyz} \in \mathbb{R}^{1\times N}$, $G_1 \in \mathbb{R}^{N\times N}$, and $G_2 \in \mathbb{R}^{N\times N}$ were previously defined in Section 8.1. The MUS-payload dynamics is given by

$$\dot{\mathbf{X}}_{SYS}^{FC} = \mathbf{A}_{SYS}^{FC}\mathbf{X}_{SYS}^{FC} + \begin{bmatrix} \mathbf{B}_{SYS,xy}^{PC} & \mathbf{0}_{2N\times 3} & \mathbf{0}_{2N\times N} \\ \mathbf{0}_{2N\times 3} & \mathbf{B}_{SYS,xy}^{PC} & \mathbf{0}_{2N\times N} \\ \mathbf{0}_{2N\times 3} & \mathbf{0}_{2N\times 3} & \mathbf{B}_{SYS,z}^{PC} \\ \mathbf{0}_{6\times 3} & \mathbf{0}_{6\times 3} & \mathbf{0}_{6\times N} \end{bmatrix}\mathbf{U}_{SYS}^{FC} + \mathbf{f}_{SYS}^{FC} \tag{60}$$

where

$$\mathbf{X}_{SYS}^{FC} = \left[\left(\mathbf{X}_{SYS,x}^{FC}\right)^T \quad \left(\mathbf{X}_{SYS,y}^{FC}\right)^T \quad \left(\mathbf{X}_{SYS,z}^{FC}\right)^T \quad \left(\mathbf{X}_{SYS,p}\right)^T \right]^T \in \mathbb{R}^{(6N+6)\times 1}, \tag{61a}$$

$$\mathbf{U}_{SYS}^{FC} = \begin{bmatrix} \sum_{j=0}^{2} G_{j,L}\frac{d^{2-j}\mathbf{Z}_{L,x,HT}}{dt^{2-j}} \\ \sum_{j=0}^{2} G_{j,L}\frac{d^{2-j}\mathbf{Z}_{L,y,HT}}{dt^{2-j}} \\ \mathbf{0}_{N\times 1} \end{bmatrix} + \begin{bmatrix} \mathbf{0}_{6\times 1} \\ \frac{d^2 z_{d,1}}{dt^2} \\ \vdots \\ \frac{d^2 z_{d,N}}{dt^2} \end{bmatrix} + \sum_{j=1}^{2} \begin{bmatrix} \mathbf{0}_6 & \mathbf{0}_{6\times N} \\ \mathbf{0}_{N\times 6} & G_j \end{bmatrix} \begin{bmatrix} \mathbf{0}_{6\times 1} \\ \frac{d^{2-j} z_{d,1}}{dt^{2-j}} \\ \vdots \\ \frac{d^{2-j} z_{d,N}}{dt^{2-j}} \end{bmatrix}^T, \tag{61b}$$

$$\mathbf{A}_{SYS}^{FC} = \begin{bmatrix} \mathbf{\Omega}_{xy}^{FC} & \mathbf{0}_{2N} & \mathbf{0}_{2N} & \mathbf{0}_{2N\times 6} \\ \mathbf{0}_{2N} & \mathbf{\Omega}_{xy}^{FC} & \mathbf{0}_{2N} & \mathbf{0}_{2N\times 6} \\ \mathbf{0}_{2N} & \mathbf{0}_{2N} & \mathbf{\Omega}_{z}^{FC} & \mathbf{0}_{2N\times 6} \\ \mathbf{\Omega}_{p,x}^{FC} & \mathbf{\Omega}_{p,y}^{FC} & \mathbf{\Omega}_{p,z}^{FC} & \mathbf{\Omega}_{p,p}^{FC} \end{bmatrix} \in \mathbb{R}^{(6N+6)\times(6N+6)}, \tag{61c}$$

$$\mathbf{B}_{SYS,xy}^{FC} = \left[\mathbf{0}_{3\times N} \quad \mathbf{I}_3 \quad \mathbf{0}_{3\times(N-3)} \right]^T \in \mathbb{R}^{2N\times 3}, \tag{61d}$$

$$\mathbf{B}_{SYS,z}^{FC} = \left[\mathbf{0}_N \quad \mathbf{I}_N \right]^T \in \mathbb{R}^{2N\times N}, \tag{61e}$$

$$\mathbf{f}_{SYS}^{FC} = \left[\mathbf{0}_{1\times(6N+5)} \quad -g \right]^T + \left[\mathbf{0}_{1\times(6N+3)} \quad -\frac{1}{m_p}\sum_{i=1}^{N} k_{\zeta_i}\mathbf{d}_{\zeta_i}^T \right]^T. \tag{61f}$$

Remark. Matrix $\mathbf{A}_{SYS}^{FC}$ is Hurwitz. Therefore, MUS-payload dynamics (60) is stable.

9. Simulation results

Consider a CALM consisting of 18 quadcopters. Each quadcopter connects to one of the grippers by a tensegrity muscle. We assume that tensegrity muscles all have the same stiffness $k_i = 50\frac{\text{N}}{\text{m}}$ and $c_i = 5\frac{\text{N·s}}{\text{m}}$. The CALM system consists of three arms. Arm 1 connects quadcopters 1, 4, 7, 8, 13, 14 to gripper O_1; Arm 2 connects quadcopters 2, 5, 9, 10, 15, 16 to gripper O_2; Arm 3 connects quadcopters 3, 6, 11, 12, 17, 18 to gripper O_3.

We simulate dynamics of CALM in the "TT", where CALM acts as moving supports. We also simulate CALM dynamic behavior, where it acts as stationary supports and controls the required reaction force.

9.1. MUS as moving support

When the MUS cooperatively carries a payload, agent coordination is defined by a continuum deformation. Continuum deformation coordination is defined by the trajectories of the leaders 1, 2, and 3 and acquired by the follower quadcopters through local communication. The graph shown in Fig. 2 defines inter-agent communication among the quadcopters. Given initial positions shown in Fig. 2, followers' communication weights, calculated using Eq. (12), are as follows:

$$w_{4,1} = w_{5,2} = w_{6,3} = w_{7,4} = w_{8,4} = w_{9,5} = w_{10,5} = w_{11,6} = w_{13,7} = w_{14,8} = w_{15,9} = w_{16,10} = w_{17,11} = w_{18,12} = 0.55.$$

The remaining communication weights are all 0.225. x and y components of the leaders' desired trajectories are assigned by solving the optimal control problem defined in Section 6.2 and formulated in [60]. Leaders initiate their motion from rest at $(X_1, Y_1) = (5.5, 0)$, $(X_2, Y_2) = (-2.5, 4)$, and $(X_3, Y_3) = (-2.5, -4)$. It is aimed that leaders reach their target destinations at

$$\left(x_{1,HT}(T_{\text{mission}}), y_{1,HT}(T_{\text{mission}})\right) = (28, 30),$$
$$\left(x_{2,HT}(T_{\text{mission}}), t_{2,HT}(T_{\text{mission}})\right) = (20, 38),$$
$$\left(x_{3,HT}(T_{\text{mission}}), y_{3,HT}(T_{\text{mission}})\right) = (20, 30)$$

in $T_{\text{mission}} = 150$ s. Note that initial area of the leading triangle is $A_0 = 32\ \text{m}^2$. The leaders' desired trajectories must satisfy equality constraint (49). x and y components of the leaders' optimal trajectories are plotted versus time in Fig. 8 (a). Followers apply the communication graph shown in Fig. 2 to acquire the desired coordination defined by leaders. x, y, and z components of follower 14 position are shown in Fig. 8 (b). Tensegrity muscle force per mass $\|\bar{\mathbf{F}}_{\text{EXT},14}\| = \|\bar{\mathbf{F}}_{\text{Muscle},14}\|$ and the magnitude of the thrust force of quadcopter 14 are plotted versus time in Fig. 8 (c).

Collision avoidance verification: We observe that quadcopters 12 and 18 has minimum separation $d_s = 0.7104$ m at $t = 0$. Quadcopter 4 is closest to the boundary $(3-1)$ of leading triangle ($d_b = 0.5792$ m) at the initial time. We assume $\epsilon = 15$ cm is the radius of a ball enclosing each quadcopter. Given d_s and d_b, $\delta_{\max}$ is computed from Eq. (46): $\delta_{\max} = \min\left\{0.5\,(d_s - 2\epsilon), d_b - \epsilon\right\} = 0.2052$. Given leaders trajectories' shown in Fig. 8 (a) and (b), eigenvalues of matrix U_D are plotted versus time in Fig. 8 (d). We choose $\lambda_{\text{CD,min}} = 0.78$ as the lower limit for the matrix U_D eigenvalues, e.g. $0.78 < \lambda_1(t) \le \lambda_2(2)$, $\forall t \ge 0$. Therefore, $\delta = \lambda_{\text{CD,min}}(\delta_{\max} + \epsilon) - \epsilon = 0.1271$ m. Inter-agent collision is avoided if $\mathcal{Y}_i - \mathcal{Y}_{i,HT} \le 0.1661$ m. In Fig. 8 (e), $\mathcal{Y}_i - \mathcal{Y}_{i,HT}$ $(\forall i \in \mathcal{V})$ is plotted versus time. It is seen that followers' continuum deformation satisfy inequality (47a); therefore, inter-agent collision is avoided. Note that the quadcopters are initially in a static equilibrium condition so that $\mathcal{Y}_i - \mathcal{Y}_{i,HT}$ is small $(\forall i \in \mathcal{V})$.

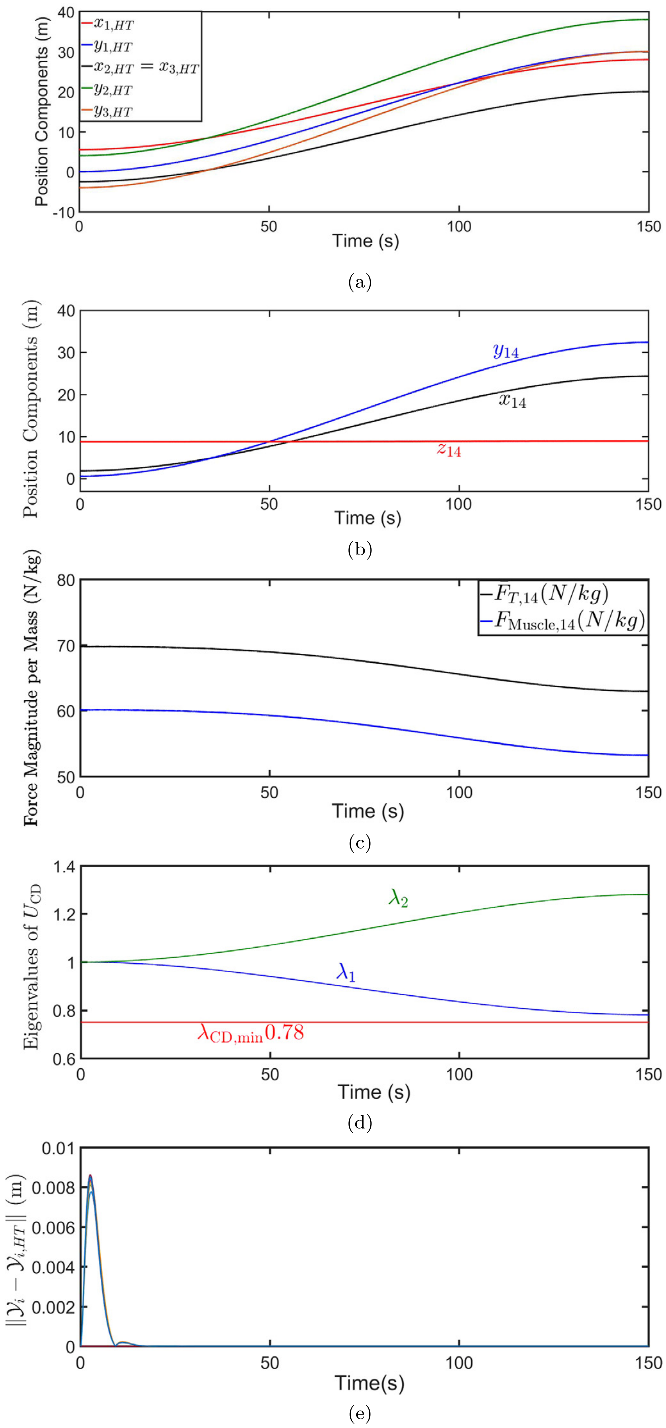

Fig. 8. (a) Leaders' desired trajectories. (b) Follower 14 position components. (c) Quadcopter 14 thrust per mass $\bar{F}_{T,14}$ and tensegrity force per mass $\|\mathbf{F}_{\text{EXT},14}\|$ vs. time. (d) Eigenvalues of matrix U_{CD} vs. time. (e) $\mathcal{Y}_i - \mathcal{Y}_{i,HT}$ vs. time ($\forall i \in \mathcal{V}$). (For interpretation of the colors in the figure(s), the reader is referred to the web version of this article.)

9.2. The MUS as a stationary support system

In this section, we assume that grippers O_1, O_2, and O_3 grasp three connection points of the payload. The payload or payload connection fixture is a triangle with mass $m_p = 100$ kg and geometry shown in Fig. 3 (b). The payload can be considered as the cap of the manipulation arms grasped at points O_1, O_2, O_3. We assume that force $\mathbf{F}_G$ and moment $\mathbf{M}_G$ are exerted on the centroid of the triangular cap.

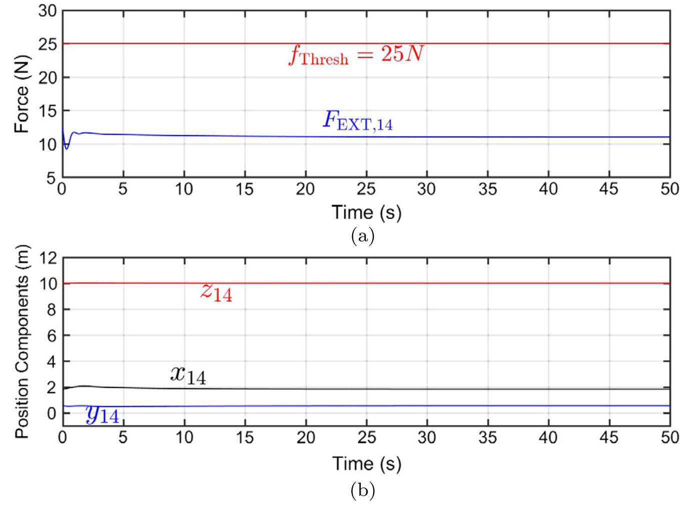

Fig. 9. (a) Tensegrity muscle force magnitude $\|F_{\text{EXT},14}\|$ vs. time. (b) Position components of quadcopter 14 vs. time.

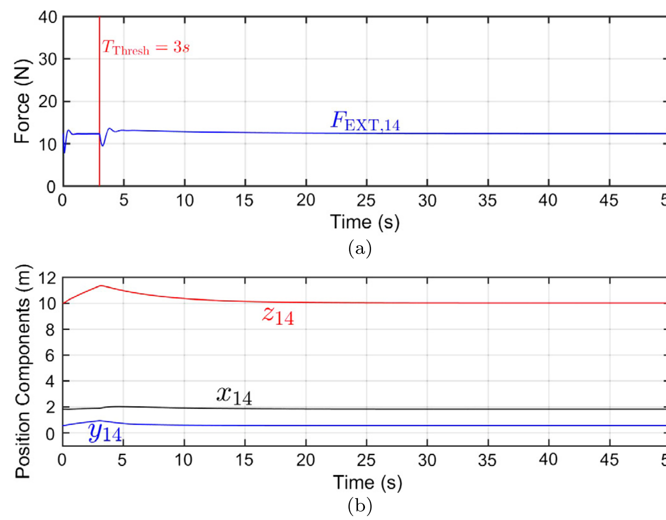

Fig. 10. (a) Tensegrity muscle force magnitude $\|F_{\text{EXT},14}\|$ vs. time. (b) Position components of quadcopter 14 vs. time.

Quadcopter initial positions are shown in Fig. 2. We consider $d_{\text{Thresh}} = 0.01$ m, $f_{\text{Thresh}} = 25$ N, $T_{\text{Thresh}} = 3$ s as the threshold distance, threshold force, and threshold time, respectively. We simulate CALM dynamic behavior for gentle and impulsive external force $\mathbf{F}_G$ and moment $\mathbf{M}_G$.

9.2.1. Gentle (smooth) external excitation

Assume that constant force $\mathbf{F}_G = [20\ 20\ 40]^T$ N and moment $\mathbf{M}_G = 0.1\mathbf{F}_G$ N.m are exerted at the centroid of the payload. In Fig. 9 (a) tensegrity muscle force $\|\mathbf{F}_{\text{EXT},14}\|$ is plotted versus time. Because $\|\mathbf{F}_{\text{EXT},14}\| < f_{\text{Thresh}} = 25$ N, the force control mode is activated. Quadcopter force controllers stabilize quadcopters at the initial destinations shown in Fig. 2. Position components of quadcopter 14 are plotted in Fig. 9 (b).

9.2.2. Impulsive external excitation

Let

$$\mathbf{F}_G = \begin{cases} [10\ 50\ 200]^T (N) & t \le 0.1s \\ 0 & \text{otherwise} \end{cases}$$

and $\mathbf{M}_G = 0.1\mathbf{F}_G$ (N.m) be exerted at the centroid of the triangular payload grasped by grippers O_1, O_2, and O_3. As shown in Fig. 10 (a) tensegrity muscle force magnitude $\|F_{\text{EXT},14}\|$ suddenly increases, causing Quadcopter 14 to activate the RBM over $t \in [0, T_{\text{Thresh}}]$. At $t = T_{\text{Thresh}} = 3s$, the quadcopter leaves the RBM because $\Psi_{T,i} := t - t_{\text{RBM}} - T_{\text{Thresh}} \le 0$ is violated, so it activates FC mode until safely returning to hover. Quadcopter 14 position time history is shown in Fig. 10 (b).

10. Conclusion

The paper has applied continuum deformation to an application in which multiple quadcopters carry a single parcel cooperatively. The cooperative payload transport mission can be accomplished in a decentralized fashion, where continuum deformation is defined by leaders and acquired by follower UAVs through local communication with less computation cost. Because continuum deformation of an MUS is scalable, a large MUS team can cooperatively carry a heavy payload without the need for a heavy-lift quadcopter design. Continuum deformation coordination also provides the ability for the team to pass through a narrow channel without collision as demonstrated in a eighteen-quadcopter case study. The proposed CALM approach can be also used in a cooperative object manipulation task, where quadcopters act as stationary supports. For this purpose, we designed a hybrid force controller to stabilize the UAV team when external forces exerted on each quadcopter are either impulsive or smooth.

Conflict of interest statement

None declared.

Appendix A

In this Appendix, we find the leaders' optimal trajectories minimizing cost function (50) and satisfying equality constraints (49). Dynamics (48) can be given in the following state-space form [57]:

$$\dot{P} = A_p P + B_p U_p \tag{62}$$

where $P = [p_i] \in \mathbb{R}^{12\times 1}$, $p_1 = x_{1,HT}$, $p_2 = x_{2,HT}$, $p_3 = x_{3,HT}$, $p_4 = y_{1,HT}$, $p_5 = y_{2,HT}$, $p_6 = y_{3,HT}$, $p_7 = \dot{x}_{1,HT}$, $p_8 = \dot{x}_{2,HT}$, $p_9 = \dot{x}_{3,HT}$, $p_{10} = \dot{y}_{1,HT}$, $p_{11} = \dot{y}_{2,HT}$, $p_{12} = \dot{y}_{3,HT}$,

$$U_p = \begin{bmatrix} u_{1,HT} & u_{2,HT} & u_{3,HT} & v_{1,HT} & v_{2,HT} & v_{3,HT} \end{bmatrix}^T$$

$$A_p = \begin{bmatrix} \mathbf{0} & I_6 \\ \mathbf{0} & \mathbf{0} \end{bmatrix}^T, \; B_p = \begin{bmatrix} \mathbf{0} \\ \mathbf{I}_6 \end{bmatrix}^T.$$

Note that $\mathbf{0}, \mathbf{I}_6 \in \mathbb{R}^{6\times 6}$ are zero-entry and identity matrices, respectively. Constraint (49) can be rewritten as [60]

$$\begin{aligned} C'_L :=& u_{1,HT}(p_5 - p_6) + u_{2,HT}(p_6 - p_4) + u_{3,HT}(p_4 - p_5) \\ &+ v_{1,HT}(p_3 - p_2) + v_{2,HT}(p_1 - p_3) + v_{3,HT}(p_2 - p_1) \\ &+ p_7(p_{11} - p_{12}) + p_8(p_{12} - p_{10}) + p_9(p_{10} - p_{11}) \\ &+ p_{10}(p_9 - p_8) + p_{11}(p_7 - p_9) + p_{12}(p_8 - p_7) = 0. \end{aligned} \tag{63}$$

Notice that constraint (63) is obtained by taking the second derivative of Eq. (49) with respect to time t. Leaders are initially at rest, and they stop within a finite horizon time T_{mission}. We assume that leaders' initial and final positions are given.

Let the cost functional (50) be rewritten in the following augmented form [60]:

$$J' = \int_0^{T_{\text{mission}}} \left\{ U_p{}^T U_p + \sigma^T (A_p P + B_p U_p - \dot{P}) + \Gamma C'_L \right\} dt \tag{64}$$

where $\sigma = [\sigma_1 \; \cdots \; \sigma_{12}] \in \mathbb{R}^{12\times 1}$ is the costate vector and Γ is the Lagrange multiplier. Using calculus of variation, X and Y components of the leaders' optimal trajectories are assigned by solving the following dynamics system:

$$\dot{S} = A_s S, \tag{65}$$

where

$$S = \begin{bmatrix} P \\ \sigma \end{bmatrix}, \tag{66a}$$

$$A_s = \begin{bmatrix} \mathbf{0} & I_6 & \mathbf{0} & \mathbf{0} \\ -\frac{1}{2}\Gamma K_1 & \mathbf{0} & \mathbf{0} & -\frac{1}{2}I_6 \\ \frac{1}{2}\Gamma^2 K_2 & \mathbf{0} & \mathbf{0} & \frac{1}{2}\Gamma K_1 \\ \mathbf{0} & -2\Gamma K_1 & -I_6 & \mathbf{0} \end{bmatrix}, \tag{66b}$$

$$K_1 = \begin{bmatrix} 0 & 0 & 0 & 0 & 1 & -1 \\ 0 & 0 & 0 & -1 & 0 & 1 \\ 0 & 0 & 0 & 1 & -1 & 0 \\ 0 & -1 & 1 & 0 & 0 & 0 \\ 1 & 0 & -1 & 0 & 0 & 0 \\ -1 & 1 & 0 & 0 & 0 & 0 \end{bmatrix}, \tag{66c}$$

$$K_2 = \begin{bmatrix} 2 & -1 & -1 & 0 & 0 & 0 \\ -1 & 2 & -1 & 0 & 0 & 0 \\ -1 & -1 & 2 & 0 & 0 & 0 \\ 0 & 0 & 0 & 2 & -1 & -1 \\ 0 & 0 & 0 & -1 & 2 & -1 \\ 0 & 0 & 0 & -1 & -1 & 2 \end{bmatrix}. \tag{66d}$$

Note that Γ in Eq. (65) can be expressed as

$$\Gamma = \frac{2\tau - \xi}{\rho}, \tag{67}$$

where

$$\begin{aligned} \rho =& (p_5 - p_6)^2 + (p_6 - p_4)^2 + (p_4 - p_5)^2 + (p_3 - p_2)^2 \\ &+ (p_1 - p_3)^2 + (p_2 - p_1)^2 \end{aligned}, \tag{68a}$$

$$\begin{aligned} \tau =& p_7(p_{11} - p_{12}) + p_8(p_{12} - p_{10}) + p_9(p_{10} - p_{11}) \\ &+ p_{10}(p_9 - p_8) + p_{11}(p_7 - p_9) + p_{12}(p_8 - p_7) \end{aligned}, \tag{68b}$$

$$\begin{aligned} \xi =& \sigma_7(p_5 - p_6) + \sigma_8(p_6 - p_4) + \sigma_9(p_4 - p_5) + \sigma_{10}(p_3 - p_2) \\ &+ \sigma_{11}(p_1 - p_3) + \sigma_{12}(p_2 - p_1) \end{aligned}. \tag{68c}$$

Moreover, optimal control inputs are obtained as follows:

$$u_{1,HT} = -\frac{1}{2}(\sigma_7 + \Gamma(p_5 - p_6)), \tag{69a}$$

$$u_{2,HT} = -\frac{1}{2}(\sigma_8 + \Gamma(p_6 - p_4), \tag{69b}$$

$$u_{3,HT} = -\frac{1}{2}(\sigma_9 + \Gamma(p_4 - p_5)), \tag{69c}$$

$$v_{1,HT} = -\frac{1}{2}(\sigma_{10} + \Gamma(p_3 - p_2)), \tag{69d}$$

$$v_{2,HT} = -\frac{1}{2}(\sigma_{11} + \Gamma(p_1 - p_3)), \tag{69e}$$

$$v_{3,HT} = -\frac{1}{2}(\sigma_{12} + \Gamma(p_5 - p_6)). \tag{69f}$$

Numerical solution: Leaders' optimal trajectories are determined by using a distributed gradient algorithm. Let $\Phi_k(t, t_0)$, P_k, and σ_k denote state transition matrix, control state, and costate at attempt $(k = 1, \; 2, \; 3, \; \ldots)$. Then [60],

$$\forall t \in [0, T_{\text{mission}}],\quad \begin{bmatrix} P_k(t) \\ \sigma_k(t) \end{bmatrix} = \Phi_k(t, t_0) \begin{bmatrix} P_k(t_0) \\ \sigma_k(t_0) \end{bmatrix} = \begin{bmatrix} \Phi_{11k}(t, t_0) & \Phi_{12k}(t, t_0) \\ \Phi_{21k}(t, t_0) & \Phi_{22k}(t, t_0) \end{bmatrix} \begin{bmatrix} P(t_0) \\ \sigma(t_0) \end{bmatrix}. \tag{70}$$

Thus,

$$P(T_{\text{mission}}) = P_k(T_{\text{mission}}) = \Phi_{11k}(T_{\text{mission}}, t_0)P(t_0) + \Phi_{12k}\sigma_k(t_0). \tag{71}$$

Notice that $P(t_0)$ and $P(T_{\text{mission}})$ are both given at initial time t_0 and final time T_{mission}. Hence, $\sigma_k(t_0)$ can be expressed as follows [60]:

$$\sigma_k(t_0) = \Phi_{12k}(T_{\text{mission}}, t_0)^{-1}(P(T_{\text{mission}}) - \Phi_{11k}(T_{\text{mission}}, t_0)P(t_0)). \tag{72}$$

Therefore, $P_k(t)$ and $\sigma_k(t)$ can be updated using Eq. (70) until

$$\forall t \in [t_0, T_{\text{mission}}],\ |\Gamma_k(t) - \Gamma_{k-1}(t)| \to 0. \tag{73}$$

References

[1] J.A. Fax, R.M. Murray, Information flow and cooperative control of vehicle formations, IEEE Trans. Autom. Control 49 (9) (2004) 1465–1476.
[2] F. Paterno, C. Santoro, S. Tahmassebi, Formal models for cooperative tasks: concepts and an application for en-route air traffic control, in: Design, Specification and Verification of Interactive Systems' 98, Springer, 1998, pp. 71–86.
[3] N. Michael, J. Fink, V. Kumar, Cooperative manipulation and transportation with aerial robots, Auton. Robots 30 (1) (2011) 73–86.
[4] D.G. Schmale Iii, B.R. Dingus, C. Reinholtz, Development and application of an autonomous unmanned aerial vehicle for precise aerobiological sampling above agricultural fields, J. Field Robot. 25 (3) (2008) 133–147.
[5] N. Michael, S. Kim, J. Fink, V. Kumar, Kinematics and statics of cooperative multi-robot aerial manipulation with cables, in: ASME 2009 International Design Engineering Technical Conferences and Computers and Information in Engineering Conference, American Society of Mechanical Engineers, 2009, pp. 83–91.
[6] A. Bazoula, M. Djouadi, H. Maaref, Formation control of multi-robots via fuzzy logic technique, Int. J. Comp. Commun. Control 3 (3) (2008) 179–184.
[7] R.M. Murray, Recent research in cooperative control of multivehicle systems, J. Dyn. Syst. Meas. Control 129 (5) (2007) 571–583.
[8] C.-L. Liu, F. Liu, Asynchronously compensated consensus algorithm for discrete-time second-order multi-agent systems under communication delay, IET Control Theory Appl. 8 (17) (2014) 2004–2012.
[9] J. Mei, W. Ren, J. Chen, Distributed consensus of second-order multi-agent systems with heterogeneous unknown inertias and control gains under a directed graph, IEEE Trans. Autom. Control 61 (8) (2016) 2019–2034.
[10] L. Zhang, C. Hua, X. Guan, Distributed output feedback consensus tracking prescribed performance control for a class of non-linear multi-agent systems with unknown disturbances, IET Control Theory Appl. 10 (8) (2016) 877–883.
[11] A. Bidram, A. Davoudi, F.L. Lewis, Z. Qu, Secondary control of microgrids based on distributed cooperative control of multi-agent systems, IET Gener. Transm. Distrib. 7 (8) (2013) 822–831.
[12] W. Ren, R.W. Beard, E.M. Atkins, Information consensus in multivehicle cooperative control, IEEE Control Syst. 27 (2) (2007) 71–82.
[13] J. Kim, K.-D. Kim, V. Natarajan, S.D. Kelly, J. Bentsman, Pde-based model reference adaptive control of uncertain heterogeneous multiagent networks, Nonlinear Anal. Hybrid Syst. 2 (4) (2008) 1152–1167.
[14] P. Frihauf, M. Krstic, Leader-enabled deployment onto planar curves: a pde-based approach, IEEE Trans. Autom. Control 56 (8) (2011) 1791–1806.
[15] K.T. Magar, M.J. Balas, D.F. Gayme, Adaptive control of inter-area oscillations in wind-integrated power systems using distributed parameter control methods, in: American Control Conference, ACC, 2014, IEEE, 2014, pp. 903–907.
[16] Y. Cao, D. Stuart, W. Ren, Z. Meng, Distributed containment control for multiple autonomous vehicles with double-integrator dynamics: algorithms and experiments, IEEE Trans. Control Syst. Technol. 19 (4) (2011) 929–938.
[17] S.J. Yoo, Distributed containment control with predefined performance of high-order multi-agent systems with unknown heterogeneous non-linearities, IET Control Theory Appl. 9 (10) (2015) 1571–1578.
[18] Z. Lin, W. Ding, G. Yan, C. Yu, A. Giua, Leader–follower formation via complex laplacian, Automatica 49 (6) (2013) 1900–1906.
[19] Y. Cao, W. Ren, Containment control with multiple stationary or dynamic leaders under a directed interaction graph, in: Proceedings of the 48th IEEE Conference on Decision and Control, 2009 Held Jointly with the 2009 28th Chinese Control Conference, CDC/CCC 2009, IEEE, 2009, pp. 3014–3019.
[20] G. Ferrari-Trecate, M. Egerstedt, A. Buffa, M. Ji, Laplacian sheep: a hybrid, stop-go policy for leader-based containment control, in: Hybrid Systems: Computation and Control, Springer, 2006, pp. 212–226.
[21] Q. Lu, Q.-L. Han, X. Xie, S. Liu, A finite-time motion control strategy for odor source localization, IEEE Trans. Ind. Electron. 61 (10) (2014) 5419–5430.
[22] H. Li, G. Chen, Z. Dong, D. Xia, Consensus analysis of multiagent systems with second-order nonlinear dynamics and general directed topology: an event-triggered scheme, Inf. Sci. 370 (2016) 598–622.
[23] S. Martinez, J. Cortes, F. Bullo, Motion coordination with distributed information, IEEE Control Syst. 27 (4) (2007) 75–88.
[24] W. Yu, P. Wang, Distributed node-to-node consensus of linear multi-agent systems with directed switching topologies, in: 2016 14th International Conference on Control, Automation, Robotics and Vision, ICARCV, IEEE, 2016, pp. 1–6.
[25] C. Li, X. Yu, W. Yu, T. Huang, Z.-w. Liu, Distributed event-triggered scheme for economic dispatch in smart grids, IEEE Trans. Ind. Inform. 12 (5) (2016) 1775–1785.
[26] L.B. Seeff, J.H. Hoofnagle, National institutes of health consensus development conference: management of hepatitis c, Hepatology 36 (5B) (2002).
[27] W. Zhao, M. Liu, J. Zhu, L. Li, Fully decentralised multi-area dynamic economic dispatch for large-scale power systems via cutting plane consensus, IET Gener. Transm. Distrib. 10 (10) (2016) 2486–2495.
[28] H. Xing, Y. Mou, M. Fu, Z. Lin, Distributed bisection method for economic power dispatch in smart grid, IEEE Trans. Power Syst. 30 (6) (2015) 3024–3035.
[29] L. Cheng, Y. Wang, W. Ren, Z.-G. Hou, M. Tan, Containment control of multiagent systems with dynamic leaders based on a $p\hat{\imath}\{n\}$-type approach, IEEE Trans. Cybern. 46 (12) (2016) 3004–3017.
[30] M. Ji, G. Ferrari-Trecate, M. Egerstedt, A. Buffa, Containment control in mobile networks, IEEE Trans. Autom. Control 53 (8) (2008) 1972–1975.
[31] W. Zhang, Y. Tang, Y. Liu, J. Kurths, Event-triggering containment control for a class of multi-agent networks with fixed and switching topologies, IEEE Trans. Circuits Syst. I, Regul. Pap. 64 (3) (2017) 619–629.
[32] W. Li, L. Xie, J.-F. Zhang, Containment control of leader-following multi-agent systems with markovian switching network topologies and measurement noises, Automatica 51 (2015) 263–267.
[33] M. Oussalah, D. Professor Ali Hessami, B. Qi, X. Lou, B. Cui, Containment control of second-order multi-agent systems with directed topology and time-delays, Kybernetes 43 (8) (2014) 1248–1261.
[34] C. Xu, Y. Zheng, H. Su, H.O. Wang, Containment control for coupled harmonic oscillators with multiple leaders under directed topology, Int. J. Control 88 (2) (2015) 248–255.
[35] K. Liu, Z. Ji, G. Xie, R. Xu, Event-based broadcasting containment control for multi-agent systems under directed topology, Int. J. Control 89 (11) (2016) 2360–2370.
[36] Y. Zhao, Z. Duan, Finite-time containment control without velocity and acceleration measurements, Nonlinear Dyn. 82 (1–2) (2015) 259–268.
[37] H. Liu, L. Cheng, M. Tan, Z. Hou, Y. Wang, Distributed exponential finite-time coordination of multi-agent systems: containment control and consensus, Int. J. Control 88 (2) (2015) 237–247.
[38] M. Bernard, K. Kondak, I. Maza, A. Ollero, Autonomous transportation and deployment with aerial robots for search and rescue missions, J. Field Robot. 28 (6) (2011) 914–931.
[39] M. Bernard, K. Kondak, G. Hommel, A slung load transportation system based on small size helicopters, in: Autonomous Systems–Self-Organization, Management, and Control, Springer, 2008, pp. 49–61.
[40] I. Palunko, R. Fierro, P. Cruz, Trajectory generation for swing-free maneuvers of a quadrotor with suspended payload: a dynamic programming approach, in: 2012 IEEE International Conference on Robotics and Automation, ICRA, IEEE, 2012, pp. 2691–2697.
[41] S. Kim, S. Choi, H.J. Kim, Aerial manipulation using a quadrotor with a two dof robotic arm, in: 2013 IEEE/RSJ International Conference on Intelligent Robots and Systems, IEEE, 2013, pp. 4990–4995.
[42] H.-N. Nguyen, S. Park, J. Park, D. Lee, A novel robotic platform for aerial manipulation using quadrotors as rotating thrust generators, IEEE Trans. Robot. 34 (2) (2018) 353–369.
[43] P.E. Pounds, D.R. Bersak, A.M. Dollar, Stability of small-scale uav helicopters and quadrotors with added payload mass under pid control, Auton. Robots 33 (1–2) (2012) 129–142.
[44] M. Bernard, K. Kondak, Generic slung load transportation system using small size helicopters, in: IEEE Intl. Conf. on Robotics and Automation, 2009, ICRA'09, IEEE, 2009, pp. 3258–3264.
[45] F.A. Goodarzi, D. Lee, T. Lee, Geometric adaptive tracking control of a quadrotor unmanned aerial vehicle on se (3) for agile maneuvers, J. Dyn. Syst. Meas. Control 137 (9) (2015) 091007.
[46] K. Sreenath, T. Lee, V. Kumar, Geometric control and differential flatness of a quadrotor uav with a cable-suspended load, in: Decision and Control Conference, IEEE, 2013, pp. 2269–2274.

[47] D. Mellinger, Q. Lindsey, M. Shomin, V. Kumar, Design, modeling, estimation and control for aerial grasping and manipulation, in: 2011 IEEE/RSJ International Conference on Intelligent Robots and Systems, IEEE, 2011, pp. 2668–2673.
[48] D. Mellinger, M. Shomin, N. Michael, V. Kumar, Cooperative grasping and transport using multiple quadrotors, in: Distributed Autonomous Robotic Systems, Springer, 2013, pp. 545–558.
[49] M. Bisgaard, A. la Cour-Harbo, J.D. Bendtsen, Adaptive control system for autonomous helicopter slung load operations, Control Eng. Pract. 18 (7) (2010) 800–811.
[50] J. Potter, W. Singhose, M. Costelloy, Reducing swing of model helicopter sling load using input shaping, in: International Conference on Control and Automation, ICCA, IEEE, 2011, pp. 348–353.
[51] S. Dai, T. Lee, D.S. Bernstein, Adaptive control of a quadrotor uav transporting a cable-suspended load with unknown mass, in: 53rd IEEE Conference on Decision and Control, IEEE, 2014, pp. 6149–6154.
[52] P.E. Pounds, D.R. Bersak, A.M. Dollar, Grasping from the air: hovering capture and load stability, in: 2011 IEEE Intl. Conf. on Robotics and Automation, ICRA, IEEE, 2011, pp. 2491–2498.
[53] Q. Jiang, V. Kumar, The inverse kinematics of cooperative transport with multiple aerial robots, IEEE Trans. Robot. 29 (1) (2013) 136–145.
[54] T. Lee, K. Sreenath, V. Kumar, Geometric control of cooperating multiple quadrotor uavs with a suspended payload, in: Decision and Control Conference, IEEE, 2013, pp. 5510–5515.
[55] G. Wu, K. Sreenath, Geometric control of multiple quadrotors transporting a rigid-body load, in: Decision and Control Conference, IEEE, 2014, pp. 6141–6148.
[56] R.E. Skelton, M.C. de Oliveira, Tensegrity Systems, vol. 1, Springer, 2009.
[57] H. Rastgoftar, Continuum Deformation of Multi-Agent Systems, Springer, 2016.
[58] W.M. Lai, D.H. Rubin, D. Rubin, E. Krempl, Introduction to Continuum Mechanics, Butterworth-Heinemann, 2009.
[59] T. Luukkonen, Modelling and control of quadcopter, Independent research project in applied mathematics, Espoo 22 (2011).
[60] H. Rastgoftar, S. Jayasuriya, Evolution of multi agent systems under a new communication topology, in: 2014 Dynamic Systems and Control Conference, American Society of Mechanical Engineers, 2014.